8-15-2018

Micro Combustion of Primary Reference Fuels in Narrow Heated Channels

Veerendra Naralasetti
Louisiana State University and Agricultural and Mechanical College

MICRO COMBUSTION OF PRIMARY REFERENCE FUELS IN NARROW HEATED CHANNELS

A Thesis

Submitted to the Graduate Faculty of the
Louisiana State University and
Agricultural and Mechanical College
in partial fulfillment of the
requirements for the degree of
Master of Science

in

Mechanical Engineering

by
Veerendra Naralasetti
B.Tech., Jawaharlal Nehru Technological University, 2016
December 2018

Acknowledgments

First and foremost, I would like to express my deepest appreciation to my faculty advisor and mentor, Dr. Ingmar Schoegl for his continuous funding and support throughout my graduate years. Special thanks for his guidance in developing LabVIEW programs and providing me the python scripts for pyrometry and HDR image processing. This work would not have been possible without his support.

I would also like to thank Dr. Shyam Menon and Dr. Manas Gartia for accepting to be in my graduate committee. I am very grateful to them for giving me helpful suggestions and advices during my weekly research meetings.

I would like to thank our sponsors U.S. Department of Energy (DOE) Office of Energy Efficiency and Renewable Energy (EERE, Bioenergy Technologies, and Vehicle Technologies Offices) for funding my work which is a part of Co-Optimization of Fuels & Engines (Co-Optima) project.

My sincere thanks to my group members: Pawan Sharma, who trained me for running the micro-reactor setup smoothly, Navid Roohani, who assisted me while conducting the experiments and his contribution in pressurized experiments, Vinicius Sauer, for his help in pyrometry and upgrading the imaging setup and Girguis Sedky, for designing the new micro reactor and his help in solving the LabVIEW issues.

Finally, I am very grateful to my parents and my brother for their immense love and encouragement.

Table of Contents

List of Tables

List of Figures

Abstract

Conventional fuel testing machines like CFR engines require large quantities of fuel. The current study seeks to overcome this limitation by introducing an alternative method using a microscale combustion reactor which consumes relatively small amounts of fuel (100-250 μl). For this reason, Primary Reference Fuels (PRF's: volumetric mixtures of n-heptane and iso-octane) which are simple surrogates of gasoline are selected to test using micro reactor. The primary goal is to determine the effectiveness of using the micro reactor setup to differentiate fuels of different octane number. Experiments with stoichiometric PRF/air mixtures are performed inside a cylindrical quartz tube of 1mm internal diameter. The fuel-air mixture velocity is varied from 5 to 80 cm/s, and three distinct combustion regimes are observed: weak flames, flames with repetitive extinction and ignition (FREI), and normal flames. In experiments, the extent of CH* chemiluminescence is captured by a monochrome machine vision camera at each set point velocity. In initial tests, wall temperature profiles are measured by a translating thermocouple setup. The experimental setup is subsequently changed to thin filament pyrometry (TFP) to allow for temperature profiles at elevated pressures. Post processing involves the extraction of flame locations to obtain ignition and extinction points. Flame temperatures are extracted from the flame locations using wall temperature profile. Different PRF blends are compared and a larger temperature difference between n-heptane and other PRFs is seen but no clear differentiation is observed from RON 50-100 at 1 atm. However, PRFs tend to show larger differences in ignition and extinction temperatures at higher pressures. To check the feasibility of the micro reactor for newly developed fuels, four fuel samples of different hydrocarbon chains with the same RON are tested in the last part of the work and results show responsiveness to octane sensitivity.

Chapter 1
Introduction

1.1 Motivation

Internal Combustion (IC) engines remain as a major power source for heavy and light motor vehicles. Due to the high energy density of hydrocarbon fuels compared to battery powered systems, IC engines still play a prominent role in the ground transportation sector. The IC engine market which started more 120 years ago, has not been replaced yet as there is no major breakthrough technology [9, 10]. Based on the ignition process, IC engines are typically categorized into Spark Ignition (SI) engine, where fuel and air mixture is ignited by a spark, and Compression Ignition (CI) engine, where injected fuel is ignited by compressed air. Petroleum derivatives such as gasoline and diesel are commonly used as fuels for SI and CI engines, respectively. Major end products after combustion are carbon dioxide and water. However, without clean combustion, other intermediate products such as carbon monoxide, particulate matter and some oxides of nitrogen and sulfur can be formed which are considered undesirable [11]. Along with harmful emissions, natural resource depletion has emerged as another global challenge due to high fuel consumption [12]. Due to these concerns, progress is being made to improve efficiency and reduce emissions. Examples include research focused on downsizing [13], lean combustion [14] and high compression ratios [15]. These research strategies necessitate a proper selection of fuel to prevent knocking [15].

Knocking is defined as a phenomenon when the end gases auto-ignite inside the combustion chamber before the spark ignition, causing a rapid pressure rise [16]. Knocking leads to less efficient performance of the engine and in the long run, causes major damage to engine parts. In 1926, Graham Edgar conducted a series of experiments with isooctane and *n*-heptane and discovered that knocking could be mitigated with the addition of isooctane to gasoline fuel. *N*-heptane possessed lower anti-knock characteristics as opposed to isooctane, which has higher knock resistance. This led to the development of the Octane Number (ON) by Russel Marker, which later became the anti-knock index for SI engine fuels [17]. Primary Reference fuels (PRFs) which are volumetric blends of *n*-heptane and isooctane are used for determining ON of fuel. Octane number is clas-

Figure 1.1: CFR engine (image source: http://www.waukeshacfr.com)

sified into Research Octane Number (RON) and Motor Octane Number (MON). RON and MON of a fuel are determined based on two testing conditions specified by the American Society for Testing and Materials (ASTM). In the RON test method (ASTM D2699), the octane rating of an unknown fuel is determined by comparing the knocking characteristics of fuel with PRF mixture in a variable compression cylinder engine called Cooperative Fuel Research (CFR engine as shown in Figure 1.1) under low load engine conditions (600 rpm and 325 K). If the fuel exhibits equivalent behavior under similar conditions along with that of PRF, the volumetric percentage of isooctane in the PRF is given as Research Octane Number (RON) of that unknown fuel [1]. For example, fuel with RON 85 and PRF 85 will possess similar knock characteristics under low loads. Under MON conditions (ASTM D2700), a similar fuel test is performed but with high load conditions with the CFR engine at 900 rpm and fuel-air temperature of 422 K at the intake [2]. The volumetric percentage of isooctane from this method is termed as Motor Octane Number (MON) of that fuel. The difference between RON and MON is termed as Octane Sensitivity (S). Apart from RON and

MON, another fuel metric called Octane Index (OI) was proposed by Kalghatgi [18] to provide the anti-knock index for different engine operating conditions. The octane Index is defined as

$$OI = RON - KS$$

where K is a constant which depends on engine condition and is assumed to be 0.5 under normal conditions [18] .

Nevertheless, RON and MON data for newly proposed fuels blends are not available due to the limitations with standard procedures [15]. CFR testing requires a large amount of fuel and for testing of newly developed fuel blend stocks such as algae derivatives [19] or green fuels, fuels may either be expensive or not be readily available in large quantities. Also, standard ASTM D2699 and D2700 tests are not applicable to fuels which are primarily oxygenated [1]. An alternative methodology needs to be developed for estimating octane numbers of advanced or limited quantity fuels.

- A simplified micro reactor setup is proposed as an alternative testing method to extract RON/MON data.
- The proposed setup should be able to differentiate various fuels of known octane number.
- Primary reference fuels are preferred since a wide range of known octane numbers can be tested using the alternative setup.
- The primary goal in this study is to determine the effectiveness of employing a micro reactor setup to characterize PRFs of various octane numbers.

To achieve the goal, PRF blends of 0, 60, 80, 90 and 100 are tested in the setup. The setup utilizes a relatively small amount of fuel sample (100-250 μl) compared to the CFR engine. Figure 1.2(a) shows the schematic diagram of a micro combustion reactor introduced by Maruta et al [20, 21, 4, 22, 23, 6]. The PRF (fuel)-air mixture enters into an externally heated quartz tube with a specified velocity and a laminar premixed flame is observed in the channel. The flame is captured using

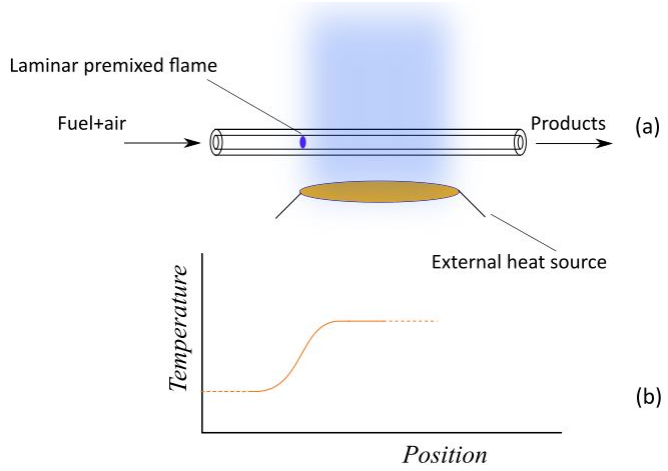

Figure 1.2: (a) Micro combustion reactor [4] and (b) axial temperature profile

a monochrome machine vision camera and an NIR sensitive camera. The temperature along the inner wall of the tube (temperature profile) is measured using a technique called multi-wavelength thin filament pyrometry [24]. Using the temperature profile, wall temperatures corresponding to each flame boundary are obtained. They are termed as T^+ and T^-. For each PRF, T^+ and T^- temperatures are compared to check the responsiveness with different octane number.

1.2 Thesis structure

The following chapter deals with the literature review and theory. Different works which employed micro reactor to observe fuel properties are addressed. In addition, several RCM and shock tube studies available on gasoline surrogates (TRFs, TPRFs, and PRFs) to predict combustion behavior are discussed. Antoine's theory of vaporization is explained to have a better understanding of fuel vaporization. As this study deals with laminar premixed flames, fuel and air should mix homogeneously prior to combustion. So, the flow rate derivation for fuel and air is presented. Last, theory and works on multi-wavelength pyrometry are discussed which is used as a method of obtaining the axial temperature profile.

Chapter 3 covers the experimental setup and standard procedure. Two versions of micro reactors are used in this study. Version 2.0 of the reactor setup (main) which uses pyrometry is explained clearly and the old reactor setup (version 1.0) is described briefly. Later parts in the chapter focus on temperature profile measurement, imaging techniques and the standard experimental procedure.

Chapter 4 presents post processing and results. This chapter gives a quick overview of post processing. In this study, various python scrips are employed, for many applications including HDR image reconstruction, temperature profile extraction from pyrometry algorithm and location extraction from image processing. Later in this chapter, results for different fuels are presented.

Chapter 5 concludes the work along with future recommendations and challenges involved with the current setup.

Chapter 2
Literature Review and Theory

2.1 Introduction to combustion and quenching

Combustion is defined as an exothermic reaction between a fuel and an oxidizer. A general stoichiometric combustion equation is given as [25]

$$1\ C_xH_y + n\ (O_2 + 3.76\ N_2) \rightarrow x\ CO_2 + (y/2)\ H_2O + 3.76n\ N_2$$

where n = x + y/4.

Here, 1 mol of fuel (C_xH_y) reacts with n moles of oxygen i.e 4.76n moles of air. The products are water and carbon dioxide.

The equivalence ratio (ϕ) of the reaction is defined as the ratio of the number of moles of air/fuel at stoichiometric conditions to the actual air fuel molar ratio, i.e.

$$\phi = \frac{(Air/fuel)_{stoich}}{(Air/fuel)} \tag{2.1}$$

If $\phi > 1$, then the mixture is called "fuel rich" or simply "rich". In contrast, the mixture will be "lean" for $\phi < 1$. Flames (continuous combustion zones) are referred to as premixed flames when the fuel air mixture is homogenized before combustion. Consider a premixed flame stabilized inside a tube. The fuel air mixture enters into the tube with a certain velocity and the flame propagates by consuming the incoming fuel-air mixture. The flame is said to be stabilized with reference to the tube when the flame velocity equals the mixture velocity.

Thermal and radical diffusions are essential for a self sustaining flame. Every fuel-air mixture has a certain range of lean-rich mixture limits called propagation limits which are controlled by heat release, rate of reaction and heat loss to the surroundings. With a gradual reduction in the tube diameter, external heat losses tend to increase, narrowing the flammability limit and at a certain diameter, the flame starts to quench as it does not release sufficient heat to compensate for heat loss and allow for propagation. The diameter below which the quenching occurs is called quenching diameter [26]. Figure 2.1 illustrates the quenching phenomenon inside the tube with a gradual

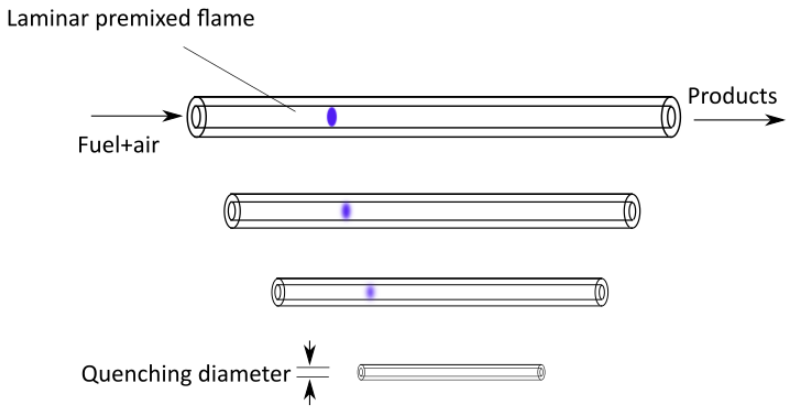

Figure 2.1: Illustration of flame quenching in narrow channels

reduction in diameter. As heat conduction and convection losses play a major role, the quenching diameter depends on preheat temperature, pressure, fuel type and equivalence ratio [26].

2.2 Literature review on micro combustion

Surface heat losses are one of the major concerns in micro scale combustion research [27]. Combustion below the flammability limits was believed impossible for so many decades. In 1954, J. H. Burgoyne, et al [28] reported that complete combustion occurs for the leanest methane air mixture with only 0.5% of methane, provided with preheating of 1000°C. Combustion below the conventional flammability limits is also shown possible with Swiss roll burners, introduced in 1974 by Lloyd, et al [29]. These are configured based on heat exchange from hot products to reactants via coil shaped narrow channels. Flame quenching under micro scale was successfully averted using heat recirculation in Swiss roll burners as demonstrated in various studies [30, 31, 32].

Along with recirculation, the extension of flammability limits is made possible with external heating. In several studies [33, 34, 6, 35, 22, 4, 36], micro combustion reactors employed external heating approaches where flames are sustained inside micro channels provided that there is a continuous supply of excess enthalpy to the reactant mixture. Micro scale reactors provide external heating to channels whose diameter are less than the quenching diameter. Under these conditions, premixed flames possess a dynamic combustion behavior which was first reported by Maruta, et al [22] in 2004. Methane-air mixtures were externally heated in a U shaped tube and periodic behavior of flame was observed at intermediate velocities under rich equivalence ratios. The flame was

reported to have an oscillatory motion with 40-60 cycles per second with ignition and extinction points. In 2005, Maruta, et al [4] observed an unstable flame phenomenon in a heated cylindrical channel with a temperature gradient. In that study [4], a tube of 2 mm diameter was heated providing a stationary temperature profile along the wall. Results showed that when fuel-air mixture velocities are varied, three different flames are observed, namely normal flame, FREI (Flames with Repetitive Extinction and Ignition) and stable weak flame.

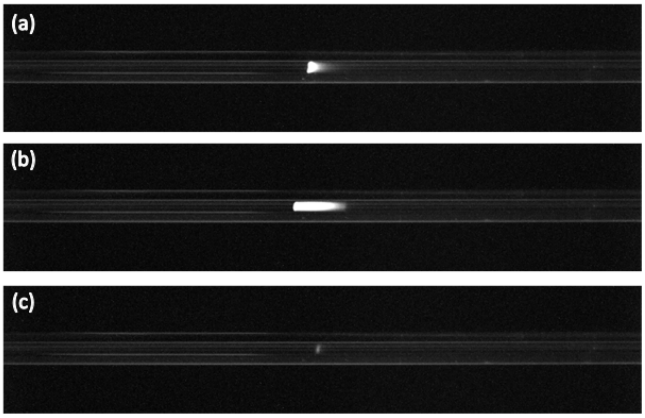

Figure 2.2: Monochromatic images of micro combustion regimes: (a) Stable (b) FREI (c) Weak

Figure 2.2 shows the raw high exposure images of various micro combustion regimes with varying tube velocities.

- At velocities higher than the laminar flame speed of a fuel, normal flames are observed which are stabilized by thermal diffusion. These are also termed as strong flames.

- At low velocities, flames possess low luminosity due to low heat release and are called weak flames. Weak flames are unable to propagate due to low heat release and they stabilize by radial heat transfer.

- At intermediate velocities, unstable flames are observed, termed as FREI (Flames with Repetitive Extinction and Ignition). In the FREI regime, the mixture ignites at a certain position called ignition point where the tube wall temperature exceeds the fuel ignition temperature. The flame front travels to the cold side consuming the incoming mixture. Volumetric heat losses occur during upstream propagation where the flame quenches at a certain

distance called extinction point. The mixture reignites at the ignition point forming a cyclic flame behavior. Due to high frequencies, the FREI region appears as a thick flame zone to the naked eye.

Using a simple micro reactor, combustion properties of various fuels were extracted [6, 35, 34, 22, 4, 20, 5, 36]. These studies primarily focused on the weak flame regime in micro reactors with a stationary temperature profile. Tsuboi, et al [5] investigated the lowest limit possible in the weak flame regime in methane air mixtures. A flat flame hydrogen burner is used for external heating and long exposures around 1-2400 seconds are used to capture weak flames due to their low chemiluminescence. No flames were observed below the flow velocity of 0.2 cm/s. Figure 2.3 (a) shows the flame positions for different flow velocities. Weak flames were observed from 1.6 cm/s to 0.2 cm/s. Figure 2.3 (a) indicates flame positions with different velocities where weak flame positions and the ignition points of FREI at 4 cm/s are located at x = 0. The results indicated that weak flame positions were closer to the ignition locations of FREI at transition velocities. It was also reported that temperature differences between weak flames and the wall surface were small. As the velocity is reduced, the temperature differences were minimized, which is shown in Figure 2.3 (b). Both flame temperature and wall temperature coincided at the lowest limit of the weak flame. The study concluded that at the lowest possible limit, weak flame temperature approaches ignition temperature of the fuel-air mixture.

Combustion properties of various gasoline surrogate components were investigated using micro flow reactors. In 2011, Yamamoto, et al [20] investigated the combustion properties of *n*-heptane in the low velocity regime. Experiments with stoichiometric mixtures of *n*-heptane and air were conducted at pressures ranging from 1-4 atm. For high pressure tests, *n*-heptane was blended with nitrogen and was vaporized beforehand. The *N*-heptane/N_2mixture was stored inside a pressurized tank. The study reported that three different luminous zones were observed simultaneously in the low velocity regime. These three zones were attributed to the three stage oxidation process of *n*-heptane. The three luminous zones were termed as the cool flame, blue flame and hot flame. At elevated pressures, the cool and blue flames were found to shift towards upstream while the hot

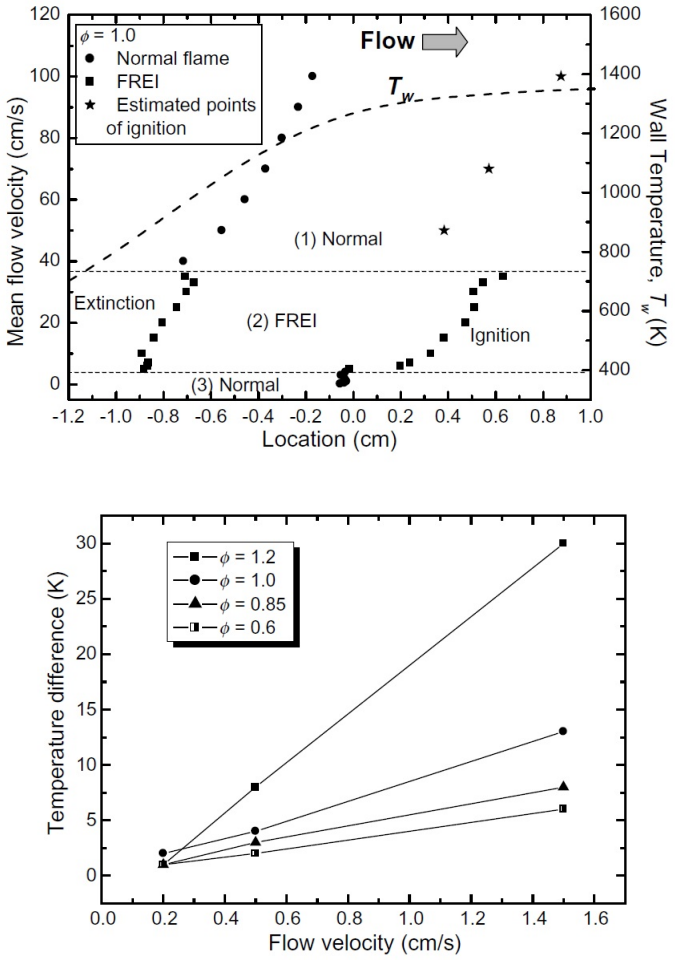

Figure 2.3: (a) flame positions at ϕ = 1.0 and (b) temperature difference between the flame and the inner surface of the tube wall at the flame position [5]

flame remained identical.

In 2011, Hori, et al [6] studied the effect of octane ratings on weak flames using PRF mixtures of 0, 20, 50 and 100 in a micro reactor setup. Figure 2.4 shows flame responses to different RON [6]. Cool, blue and hot flames can be seen for PRF 0 which agreed with the previous study [20]. However, cool flames (enclosed in dotted lines) were absent in the isooctane case. The test indicated that hot flames shifted towards the high temperature region with an increase in the octane number whereas cool flames gradually disappeared. In the following year, Hori, et al [35] performed similar tests with *n*-heptane and toluene blends. Results showed a shift in weak flames positions with an addition of toluene. The hot flame shifted towards the high temperature region (downstream) with an increase in toluene content indicating its ignition inhibition effect.

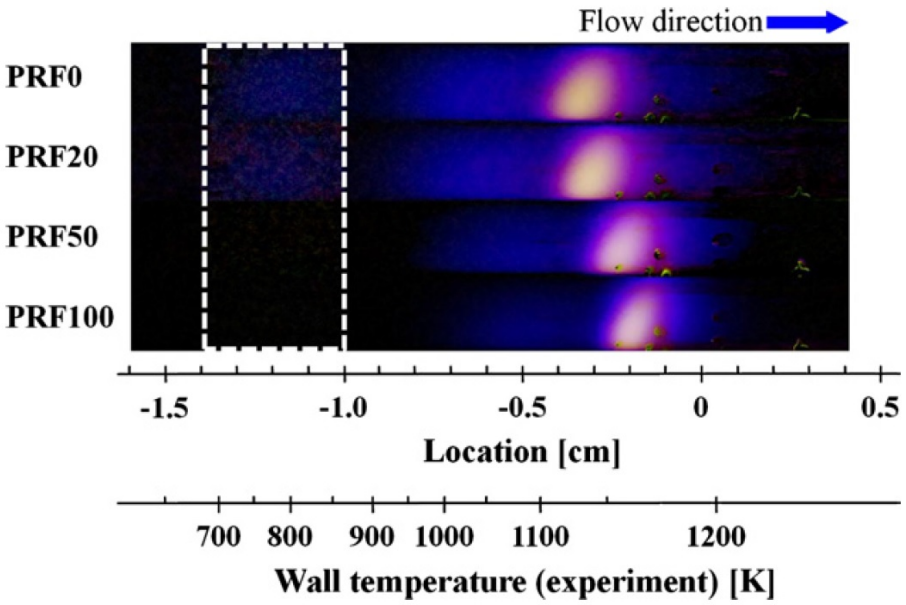

Figure 2.4: Weak flame positions w.r.t RON [6]

Similar experiments concentrating on the weak flame region were performed by Suzuki, et al [36] in 2013, with different diesel surrogates and reported that the weak flame position moved to the cold side with higher cetane numbers. Kamada, et al [23] observed weak flame responses for different natural gas components such as methane, ethane, propane, and n-butane. Computational results indicated a linear relationship with RON of the fuel and its weak flame position. However, experimental results at 1 atm showed a non-monotonic relationship of flame positions to RON. Combustion flame regimes were also reported by Di Stazio, et al [37] in 2016, with a burner configuration where symmetric heating is provided with the help of three torches separated by 120° with each other. In 2018, a vertical type micro reactor was introduced by Grajetzki, et al [38] to study the reactivity of PRF mixtures at ultra lean conditions This study reported that weak flames shifted towards upstream when the equivalence ratio is reduced from 1 to 0.5 indicating higher reactivity at low temperature region.

Based on this literature review, there is a strong evidence that fuels can be characterized using a micro reactor system. The wall temperature near the lower limit of a weak flame corresponds to the fuel ignition temperature [5]. The weak flame locations are shown sensitive based on the combustion characteristics of fuels such. Weak flame locations are also shown sensitive with different

octane [23, 6, 38] and cetane numbers [36]. Though there are results on PRFs focusing on the weak flame region, the flame responses with RON in the stable flame and in the FREI region are still unclear. It is also uncertain whether fuels with different octane sensitivities can be distinguished using a micro reactor. Therefore, the goal is to observe ignition characteristics in all three flame regimes for fuels with different RON and octane sensitivity.

2.3 Ignition delay and octane number correlations

For gasoline-like fuels, MON is usually less than RON. This is attributed to the Negative Temperature Coefficient (NTC) behavior of alkanes at higher temperatures [39]. The NTC behavior is defined as a condition when the auto-ignition delay of a fuel-air mixture either increases or show an inflection instead of decreasing with higher inlet temperatures [40]. NTC behavior is exhibited by alkanes (such as *n*-heptane and isooctane) at higher temperatures [39]. At MON conditions, the fuel air inlet temperature is higher compared to RON conditions while testing in a CFR engine [2]. PRFs which are binary alkane mixtures, exhibit NTC behavior in MON tests unlike during RON tests. While the NTC behavior causes increased ignition delay, higher compression is required for engine knock with PRFs. However, gasoline type fuels have olefins and aromatics, which do not display NTC behavior at MON conditions. This means unlike at RON conditions, higher compression is required for PRF than tested fuel at MON conditions [39]. So, at respective compression of that fuel, PRF with lower octane number will be matched, thus giving a lower value for MON. The difference between RON and MON is defined as Octane Sensitivity (S). For gasoline fuels, octane sensitivity usually ranges from 10-20 [39, 41]. PRFs by definition have an octane sensitivity of zero. Thus, Toluene is added to *n*-heptane to PRF to acquire the missing sensitivity component and this type of gasoline surrogate is called Toluene Standard Fuel (TSF) or Toluene Reference Fuel (TRF).

Apart from micro reactor experiments, ignition properties of gasoline surrogates were also studied using shock tubes and rapid compression machines (RCM). Ignition delay time (IDT) in these experiments are determined from time histories of temperature, pressure or species composition. Fieweger, et al [42] in 1997, conducted series of shock tube experiments with different PRFs

and concluded that ignition delay time was increased and the extent of NTC region is reduced as octane numbers increased. Tanaka, et al [43] developed an RCM model for PRF mixtures to predict knock, ignition delays and burning rates. Several other RCM and shock tube tests are performed on TSFs and PRFs to calculate ignition delays at different pressures and temperatures [44, 45, 46, 47, 48, 49].

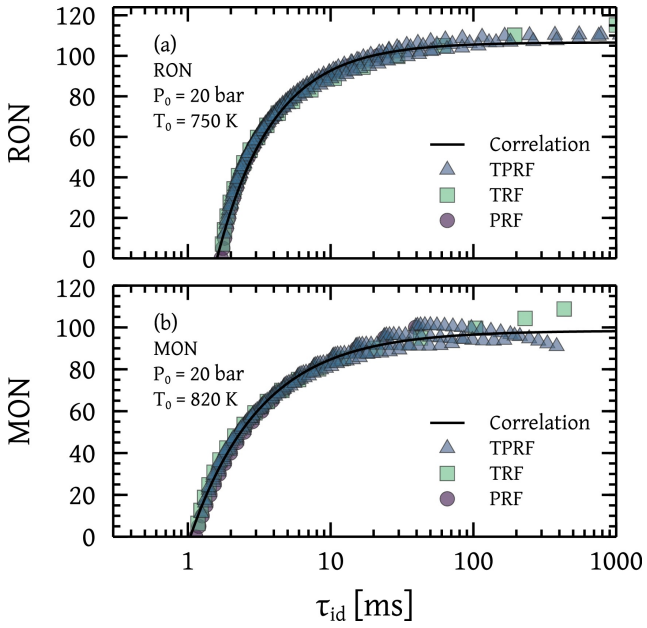

Figure 2.5: IDTs of different surrogates and correlated model at 20 bar [7]

Several efforts have been made to understand the relationship between octane number (ON) and ignition delay time (IDT). In 1997, Griffiths, et al [50] measured IDTs in rapid compression machines over a wide range of PRFs and was not successful in correlating higher octane numbers to IDTs. Instead, they suggested employing auto-ignition temperatures of PRFs to link with their ON. Naser, et al [51] successfully predicted RON and MON of actual fuels using an Ignition Quality Tester (IQT). An IQT consisting of a constant volume combustion chamber with liquid spray was used for measuring IDTs. The ignition delay time is measured from the period between fuel injection to ignition. IDTs are obtained for different PRFs and TRFs at different temperatures under the same pressure. A correlation was obtained based on octane index (OI) and ignition delay, thereby extracting RON and MON from unknown fuels based on IDTs. The resulting RON and MON values were then compared with actual values and the uncertainties are very low. In their

continuing work [7], octane numbers were predicted based on the simulated ignition delay curve generated with a wide range of PRF mixtures. Figure 2.5 shows an IDT model obtained with PRFs at 20 bar at RON and MON condition. Using this model, octane numbers of different surrogates were estimated from their ignition delays.

2.4 Liquid flow rate derivation

In this study, the homogeneous mixture is maintained at the desired equivalence ratio and the flow rates of liquid and air should be adjusted according to different flow velocities inside the channel. In this section, both air and liquid flow rate formulas are derived from the desired set points in the micro reactor. It is assumed that the fuel-air mixture is flowing with a velocity v in a channel of cross section area A, maintaining the given equivalence ratio of ϕ. A general stoichiometric combustion equation of 1 mol of fuel (CxHy) with n moles of air is given as [25]

$$1\ C_xH_y + n\ (O_2 + 3.76\ N_2) \rightarrow x\ CO_2 + (y/2)\ H_2O + 3.76n\ N_2$$

where n = x + y/4

For combustion with equivalence ratio ϕ, assume 1 mole of fuel reacts with k moles of air. The equation will be

$$1\ C_xH_y + k\ (O_2 + 3.76\ N_2) \rightarrow x'\ CO_2 + (y'/2)\ H_2O + 3.76k\ N_2$$

From the definition of equivalence ratio [25]

$$\phi = \frac{(Air/fuel)_{stoich}}{(Air/fuel)} \tag{2.2}$$

Substituting fuel and air moles from both combustion equations yields

$$\phi = \frac{n/1}{k/1}$$

$$k = \frac{n}{\phi} \tag{2.3}$$

The total volumetric flow rate$\left(\dot{Q}_T\right)$ inside the tube is

$$\dot{Q}_T = A.v \tag{2.4}$$

As reactants consists1 mol of fuel and k moles of air. The volumetric flow rate of air $\dot{Q}_{air}$ is

$$\dot{Q}_{air} = \frac{k}{1+k}\dot{Q}_T$$

Substituting k from Eq. 2.3 gives

$$\dot{Q}_{air} = \frac{n}{\phi+n}\dot{Q}_T \tag{2.5}$$

Next, it is considered that the total volumetric flow rate of the mixture is the sum of flow rates of air $\dot{Q}_{air}$ and fuel vapor $\dot{Q}_{vapor}$

$$\dot{Q}_T = \dot{Q}_{air} + \dot{Q}_{vapor} \tag{2.6}$$

Substituting $\dot{Q}_{air}$ from Eq 2.5 in Eq. 2.6 and solving for $\dot{Q}_{vapor}$ gives

$$\dot{Q}_{vapor} = \dot{Q}_T - \dot{Q}_{air}$$

$$\dot{Q}_{vapor} = \frac{\phi\dot{Q}_T}{\phi+n} \tag{2.7}$$

As the fuel will be in liquid state initially, the volumetric flow rate in liquid state, $\dot{Q}_{liq}$ needs to be determined. As the total mass flow rate of fuel will be equal in both vapor and liquid phases,

$$m_{liq} = m_{vapor}$$

$$\rho_{liq}\dot{Q}_{liq} = \rho_{vapor}\dot{Q}_{vapor}$$

$$\dot{Q}_{liq} = \frac{\rho_{vapor}}{\rho_{liq}}\dot{Q}_{vapor}$$

$$\dot{Q}_{liq} = \left(\frac{\rho_{vapor}}{\rho_{liq}}\right)\frac{\phi}{\phi + n}\dot{Q}_T \tag{2.8}$$

where ρ_{liq} and ρ_{vapor} are the liquid and vapor densities of the fuel. Assuming ideal gas state for fuel vapor i.e,

$$\rho_{vapor} = \frac{P}{RT}$$

Substituting ρ_{vapor} in Eq. 2.8 gives

$$\dot{Q}_{liq} = \left(\frac{P}{RT\rho_{liq}}\right)\frac{\phi}{\phi + n}\dot{Q}_T \tag{2.9}$$

In experiments, the pressure (P) inside the flow channel is maintained at 1 atm. The temperature (T) of the vapor is assumed to be at room temperature. For each fuel, the liquid density is known. The total volumetric flow rate ($\dot{Q_T}$) can be calculated by substituting flow velocity (v) and the cross section area (A) of the quartz tube. All fuel tests are conducted at stoichiometric conditions, hence the equivalence ratio (ϕ) is 1. The number of moles of air required for ideal combustion (n) can be found for each fuel from balancing the combustion equation. Table 2.1 shows liquid flow rates of n-heptane for different velocities at 1 atm in a channel of 1 mm internal diameter. The volumetric flow rates range from 0-5 μl/min for the mixtures velocities ranging from 0 to 80 cm/s. Hence, based on fuel rates, syringes of 100 μl are selected as an appropriate choice for fuel delivery.

Table 2.1: Flow rates for n-heptane

Velocity (cm/s)	10	20	40	60	80
Phi (ϕ)	$\dot{Q}_{liq}$ (μl/min)	$\dot{Q}_{liq}$ (μl/min)	$\dot{Q}_{liq}$ (μl/min)	$\dot{Q}_{liq}$ (μl/min)	$\dot{Q}_{liq}$ (μl/min)
0.6	0.329	0.658	1.317	1.976	2.635
0.8	0.437	0.875	1.750	2.625	3.501
1	0.544	1.089	2.179	3.269	4.359
1.2	0.651	1.303	2.606	3.909	5.212
1.4	0.757	1.514	3.029	4.543	6.058
1.6	0.862	1.724	3.449	5.173	6.898

2.5 Antoine's equation

As this study mostly focuses on liquid fuels, the fuel needs to be converted into the gaseous state before being introduced into the micro reactor. Previous studies [6, 35, 20] stored liquid fuels by

pre-vaporizing and blending with nitrogen inside a compressed cylinder for high pressure experiments. However, this process is limited by the fuel's vapor pressure inside the tank. Moreover, this process requires mass flow controllers compatible with isooctane and *n*-heptane. Instead, fuel in the liquid state is delivered according to the desired flow rates at user defined set points (refer section 2.4) using a programmable syringe pump. The fuel is vaporized with co-flowing air inside a mixing chamber and vaporization is expected based on Antoine's equation of vapor pressures [52]. The equation is obtained from the Clausius-Clapeyron relation, first formulated by Louis Charles Antoine in 1888. The equation is used to obtain vapor pressures of pure fuels for given temperatures as

$$\log P = A - \frac{B}{C+T} \tag{2.10}$$

where A, B, and C are constants related to the fuel of interest, T is the temperature (K) and P is the vapor pressure (bar). The constants are, however, not the same for the entire range of temperature range. Usually for temperatures above 350 K, another set of A, B and C values will be used. The equation can be rewritten as

$$T = \frac{B}{A - log_{10}P} - C \tag{2.11}$$

This relation is termed as August equation to obtain the temperature (T) required for complete evaporation.

For example, A, B, and C for isooctane are 3.94736, 1282.332, and -48.444 respectively [53]. For a stoichiometric combustion equation for 1 mol of isooctane can be written as

$$1\ C_8H_{18} + 12.5\ (O_2 + 3.76\ N_2) \rightarrow 8\ CO_2 + 9\ H_2O + 47\ N_2$$

The homogeneous reactant mixture comprises of 1 mol of isooctane with 12.5×4.76 mol of air. The partial pressure (bar) of isooctane for the mixture at 1 atm is

$$P_{isooctane} = \frac{1}{1 + 12.5(1 + 3.76)} \times 1.01325$$

$$= 0.0167 \text{ bar}$$

At room temperature, Substituting A, B, and C in Eq. 2.10, the vapor pressure for isooctane is

$$\log P = 3.94736 - \frac{1282.332}{-48.444 + 298}$$

$$P = 0.0644 \text{ bar}$$

Hence isooctane will be in the vapor phase at room temperature as the partial pressure in the mixture is less than the vapor pressure.

The fuel vaporisation can also be explained using August relation. Substituting A,B,C and $P_{isooctane}$ in Eq. 2.11, the temperature required for vaporization of the mixture will be 272 K, which is less than room temperature.

Similarly, for *n*-heptane, constants are 4.81803, 1635.409, and -27.338 respectively [54]. Substituting in August equation results in the vaporization temperature of 277 K which is also less than room temperature. From both *n*-heptane and isooctane results, it is implied that heating is not necessary for PRF mixtures inside the mixing unit as the partial pressures are less than the saturated vapor pressures.

2.6 Thin filament pyrometry

The final outcomes from this study are flame locations and wall temperatures based on flame locations. Hence, temperature measurements play a crucial role in the current study. In the previous works mentioned in Section 2.2, all temperature measurements are performed using a K- type thermocouple in the hot channel. However, thermocouple measurements are limited to single point measurements, thus requiring translation for obtaining temperature profiles. Uncertainties associated with thermocouple measurements include conduction and radiation errors at larger diameters which need to be corrected to obtain accurate results. Further at high flame temperatures, thermocouples used are platinum based which is an excellent catalyst. To avoid catalysis from platinum, inert material needs to be coated on the thermocouple junction.

Thin filament Pyrometry is preferred over thermocouple due to its greater degree of freedom inside the micro channel. Pyrometry is a good choice as the measurements involve in radiative heat

transfer and the target size can either be a single point or a wide region. Pyrometry can be explained simply by the Plank's law of spectral distribution. Any substance or matter at a given temperature emits radiation a characteristic spectrum [55]. According to the Plank's law, spectral intensity per unit solid angle (W $sr^{-1}m^{-1}$) of a blackbody at temperature T at wavelength λ is given by [55],

$$I_{\lambda,b}(\lambda,T) = \frac{2hc_o^2}{\lambda^5\left(\exp\left(hc_o/\lambda K_B T\right)-1\right)} \tag{2.12}$$

where h, k_B are Plank's and Boltzmann constants, which are 6.626×10^{-34} Js and 1.381×10^{-23} J/K, respectively and $c_o = 2.9 \times 10^8$m/s is the speed of light. Substituting the constants, the equation can be written as

$$I_{\lambda,b}(\lambda,T) = \frac{C_1}{\lambda^5\left(\exp\left(C_2/\lambda T\right)-1\right)} \tag{2.13}$$

in which $C_1 = 1.191 \times 10^{-16}$W $m^2$and $C_2 = 1.439 \times 10^{-2}$m K

In case of a real surface with emissivity $\varepsilon(\lambda,T)$, the plank equation is written as

$$I_{\lambda}(\lambda,T) = \frac{\varepsilon C_1}{\lambda^5\left(\exp\left(C_2/\lambda T\right)-1\right)} \tag{2.14}$$

Equation 2.14 can be used to determine the temperature of a surface if the value of emissivity (ε) is known. This is the fundamental concept in pyrometry technique. It estimates the temperatures based on the spectral emissions from the target surface. In the case of multi wavelength pyrometry, emissivity values are not necessarily required for estimating temperatures.

In 1987, Vilimpoc, et al [56] estimated the temperatures of a filament within the range of 1000 - 2600 K. They termed this method as thin filament pyrometry (TFP) where a small 15 μm ceramic filament made of Silicon Carbide (SiC) was placed in a hot flow field for temperature measurement. SiC fiber is chosen due to its high emissivity with small variance with temperature and relatively low conductivity. In their study, the emissivity value is assumed to be constant and filament emissions were detected using InGaAs sensor. Calibration measurements of total emission values were done initially with known temperatures. Filament temperatures were estimated

by correlating the total emissions with the calibration curve. The results showed an uncertainty of 80 K in the lower temperature region. Later in 1993, Pauzin, et al [57] extracted temperature profiles in premixed flames using TFP. They reported reduced uncertainties when the sensor is replaced with an infrared camera. Pyrometry measurements were also done using a digital camera of high resolution by Maun, et al [58] and reported an uncertainty of $\pm$60 K. All the aforementioned studies [56, 57, 58] used calibration measurements and a known value of emissivity. Pyrometry is also shown possible without estimating the emissivity (ε) with dual [59, 60, 61, 62] or multi wavelength pyrometry methods [63, 64, 24]. Pyrometry results were also shown to be improved by using high dynamic range (HDR) images instead of low dynamic range images (LDR) due to better sensitivity, signal to noise ratio and extended temperature ranges [61].

The present work utilizes thin filament-multi wavelength pyrometry developed by Sauer, et al [24] as a measurement tool without any requirement of a calibration measurement. The emissions are captured using a near-infrared camera with a CMOS sensor. The images captured at different exposures are converted to HDR images using the Debevec reconstruction algorithm [65]. The temperatures are obtained by solving a linear system of emission equations obtained at each wavelength. More details of this method are explained in [24].

Chapter 3
Experimental Methods

3.1 Introduction

This study involves investigating laminar premixed flames. The fuel is a PRF blend in the liquid state which needs to be converted into the vapor phase. Further, the vapor should homogeneously mix with air at a defined equivalence ratio prior to combustion. This is achieved using a co-flow vaporization unit.

The fuel-air mixture is sent into a micro channel and flame regimes (stable, FREI and weak flames) need to be observed at different mixture velocities. This is possible only if the channel diameter is less than the quenching diameter. Hence, a micro reactor unit with a quartz tube of 1 mm internal diameter is chosen, which is less than the quenching diameter (2-3 mm at 1 atm [26]).

Images of flames (stable, FREI and weak) in the channel need be captured and temperature profiles need to be estimated to obtain T^+ and T^- temperatures. This is attained using an imaging unit where the flames are captured using a dual camera setup. The imaging unit is also employed to capture a silicon carbide fiber (SiC) to measure wall temperature profile. Overall, the setup can be divided into three parts:

1. Vaporization unit - mixing and vaporization
2. Micro reactor unit - external heating and micro-combustion
3. Imaging unit - capturing of flame and filament images

Each unit in the setup is explained in the following sections. Standard procedures for fuel preparation, running the setup, and taking of measurements are explained in the last section.

3.2 Vaporization unit

Figure 3.1 shows a schematic of the vaporization unit. A gas tight syringe (Hamilton 1710; 1000 psig) of 100 μl capacity is loaded with a PRF blend. The fuel is delivered into a brass block chamber by means of an automatic syringe pump (Chemyx OEM; 0.001 μL/min to 60 mL/min)

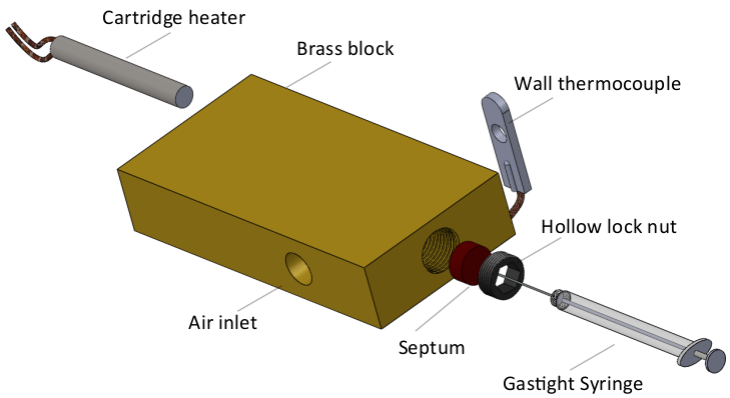

Figure 3.1: Vaporization unit (disassembled)

and the fuel flow rate is controlled using a LabVIEW program. To prevent leakage, a silicone rubber septum (3/8" thick) is used as a stopper at the inlet of the unit and a hollow lock nut is fastened to seal the inlet. A syringe needle is pierced through the septum into the block and the fuel is injected from the tip. Air from a compressed cylinder is dispatched into the unit and the flow rate is adjusted using a mass flow controller (Cole-Palmer; 1-100sccm, 32907-61). Fuel and air from different passages mix and co-flow along a single channel towards the outlet. The fuel vaporizes in the co-flow mixture according to Antoine's equation of vapor pressures. As discussed in Section 2.5, heating is not required for vaporizing PRFs as their partial pressures in the mixture will be less than the saturated vapor pressure. However, to ensure rapid vaporization, heating is provided to the gasoline representative fuels tested in this study. The block is heated to a temperature higher than the vaporization temperature obtained from Antoine's equation. A cartridge heater is inserted into the brass block to heat the unit and a K-type surface thermocouple is attached to the brass block to control the temperatures. Both heater and thermocouple are wired in a control circuit and the heat supply from the cartridge heater is automatically adjusted according to the thermocouple readings.

3.3 Micro reactor unit (current version, v2.0)

The micro reactor unit consists of a quartz tube of 1 mm internal diameter arranged between two manifolds and a burner for external heating. Figure 3.2 shows the schematic of the micro reactor unit. A flat flame Mckenna burner (Holthuis & Associates, bronze plug) burner is employed to produce a steady temperature profile inside the tube. Hydrogen is chosen as fuel for the burner to have a better visualization of flames inside the tube. Air is delivered to the burner from a

compressor whereas hydrogen is supplied from a compressed cylinder. Two mass flow controllers (Cole Palmer; 1-100 slpm, 2.5-250 slpm) are used to regulate hydrogen and air flow rate to the burner. Along with the hydrogen-air inlet, water is used in a cooling circuit to cool the burner plug. An R-type thermocouple is placed above the burner's surface to monitor the external temperature.

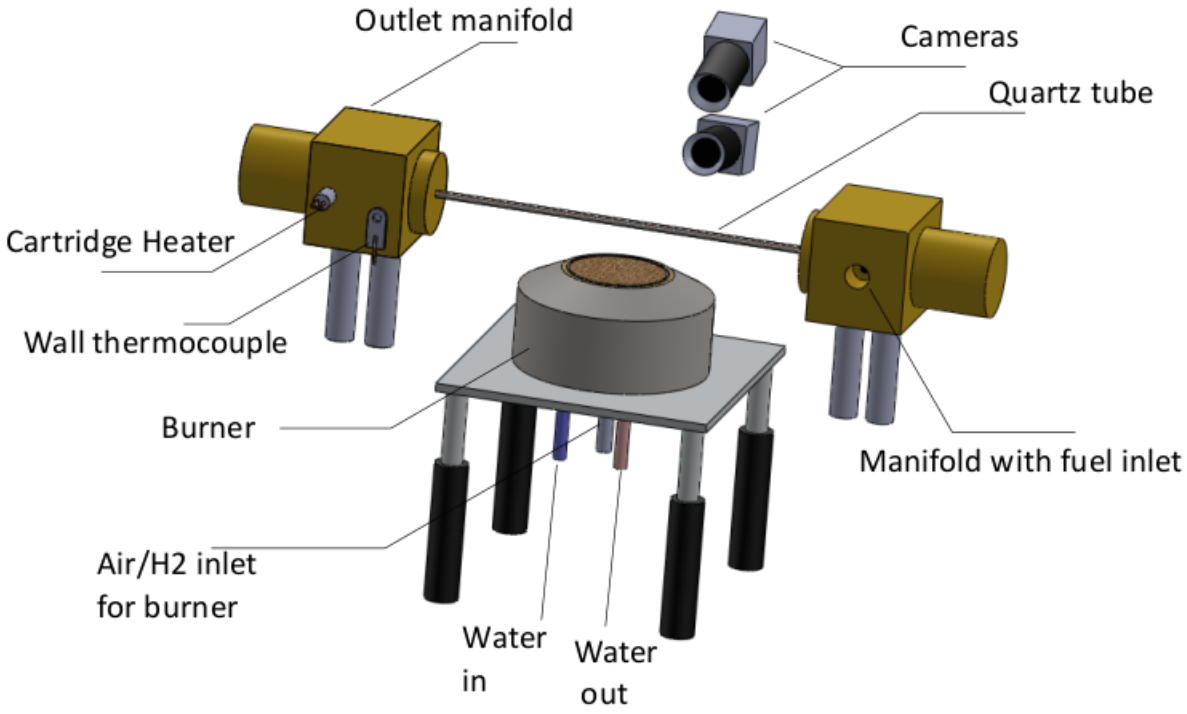

Figure 3.2: Micro reactor unit (v2.0) with the burner

A 1mm internal diameter quartz tube of 21.5 cm length is placed 30 mm above the burner. The tube is secured inside the manifolds using a circular brass disk with an O-ring connection to provide a leak free passage from the manifold to the tube. A 76 μm silicon carbide (SiC) fiber is placed inside the tube where the two fiber ends emerge from the manifolds. Two positioner units are clamped to both ends of the SiC fiber. The positioners provide for a means to adjust the fiber in any radial direction inside the tube. To avoid sagging of the fiber due to thermal expansion, two tension springs are placed inside the positioner setup to keep the fiber in tension. After adjusting the filament to the top position inside the quartz tube, the positioner units are closed with sealing cups. The end products inside the tube condense at the exit manifold and it may lead to fuel flow fluctuations. In order to avoid condensation, a cartridge heater with a control circuit is used to heat the exit manifold and a wall thermocouple is placed to check the temperatures. Though all

fuel tests done in this study are at atmospheric pressure, the micro reactor is designed to withstand higher pressures up to 10 atm [8]. The outlet manifold has openings for accessories to control the outlet flow and to adjust the pressure inside the tube.

3.4 Imaging unit

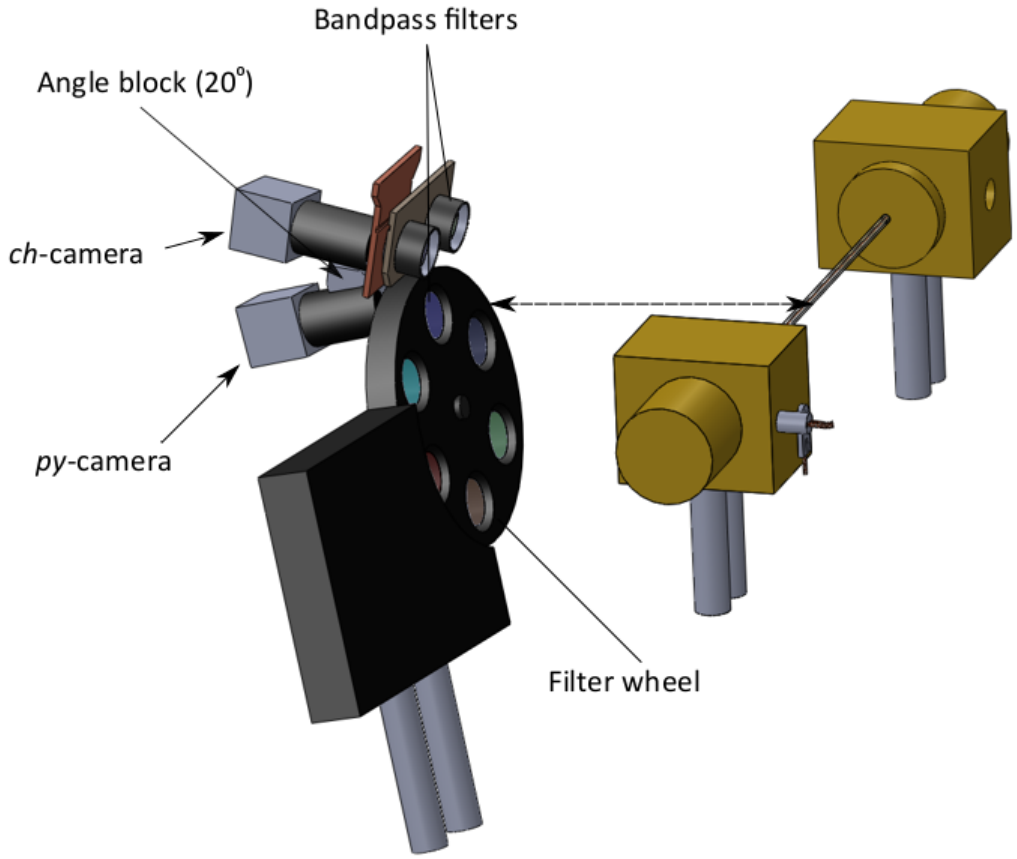

Figure 3.3: Camera setup

Imaging is performed using two monochrome machine vision cameras equipped with different band pass filters. Figure 3.3 shows the dual camera setup directing towards the micro reactor. The first camera located on top is employed to capture chemiluminescence of the flame inside the tube. The first camera is termed chemiluminescence camera (*ch*-camera). As weak flame intensities are low, a lens with a large aperture (f/1.4) is chosen. Based on the wavelength range of CH* chemiluminescence, 394nm and 430nm band pass filters are attached to a dual position slider (Thorlabs ELL6K). The slider is used for switching the two filters in a linear motion driven by a piezo-electric motor. The slider is attached to the *ch*-camera.

The second camera, located at the bottom, is used to capture the SiC filament to obtain the temperature profile using multi wavelength pyrometry. This camera is termed pyrometry camera (*py*-camera). Six different band pass filters with 435, 650, 750, 850, 950, and 1050 nm are used for pyrometry measurements. They are placed inside a 6-position filter wheel (Thorlabs FW102C) to switch to different filter positions by wheel rotation. The filter wheel is attached to the *py*-camera. To limit chromatic aberration from measurements with different filters, the f-stop value is set to 5.6 in the bottom camera. As both cameras should focus on the same filament, two angular blocks of 16° and 4° (Thorlabs AM16C, AM4C) are mounted between the two cameras. The selection of angle blocks is based on the distance between the tube and the camera setup which is 18 cm in this study. Distance rings are added if the focal range is insufficient.

All images are captured in multiple exposure sequences to obtain a composite High Dynamic Range (HDR) image in post processing [24]. Table 3.1 gives the parameters chosen for multiple imaging sequences. All the filter slider, wheel, and dual camera operations are controlled using a single LabVIEW program with a USB interface. The LabVIEW program is designed to capture continuous imaging sequences at each filter, starting with the pr-camera, followed by the ch-camera. The sequence starts with the lowest exposure of 0.125 ms and the exposure is multiplied by the factor of 2 with each image. The maximum exposure is 2000 ms and the total number of images is 15. All these 15 low dynamic range images with different exposures are reconstructed into a single composite HDR image later in the post processing step.

Table 3.1: Imaging parameters

Parameter	Value
Minimum exposure	0.125 ms
Maximum exposure	2000 ms
Sequence	0.125, 0.250, 0.5, 1, 2, 4,....,1024, and 2000ms
Total image count	15
Camera Gain	1x
Pixel clock	20
Resolution	1280 x 256
Shutter mode	Global

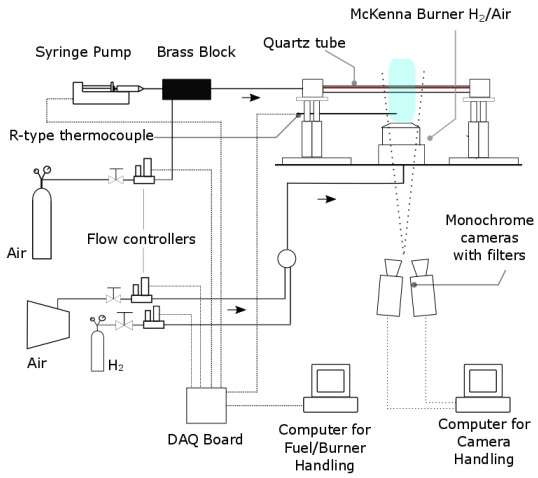

Figure 3.4: Schematic line diagram

3.5 Instrument control

Figure 3.4 shows the schematic line diagram of the experimental setup. The setup consists of different electronic devices such as mass flow controllers (MFCs), an automatic syringe pump and monochrome cameras, filter wheel, external thermocouple, and slider. Two computers operate all these devices simultaneously while running the experiment via a data acquisition board (DAQ) or directly through a USB connection. The first computer is used for handling MFC signals, syringe pump commands, and thermocouple readings. A DAQ system is attached to the first computer and the operations are controlled through a LabVIEW program. The volumetric flow rate formulas $\dot{Q}_{air}$ and $\dot{Q}_{liq}$ (refer to Section 2.4) are scripted in the block diagram code of the flow controller LabVIEW program with the mixture velocity 'v' given as an input parameter. With each velocity set point, the mass flow controller for air and syringe pump for fuel automatically adjust to deliver appropriate amounts to maintain the desired equivalence ratio. The second computer with another LabVIEW program is connected to the dual camera setup and is used to operate the imaging sequence.

3.6 Micro reactor unit (older version, v1.0)

One of the key differences between the old setup and the new one is the wall temperature measurement system. In the older version, a K-type thermocouple (Omega KMTXL, 0.25mm diameter) is used to acquire the temperature profile. Figure 3.5 shows the schematic of the older version. Ther-

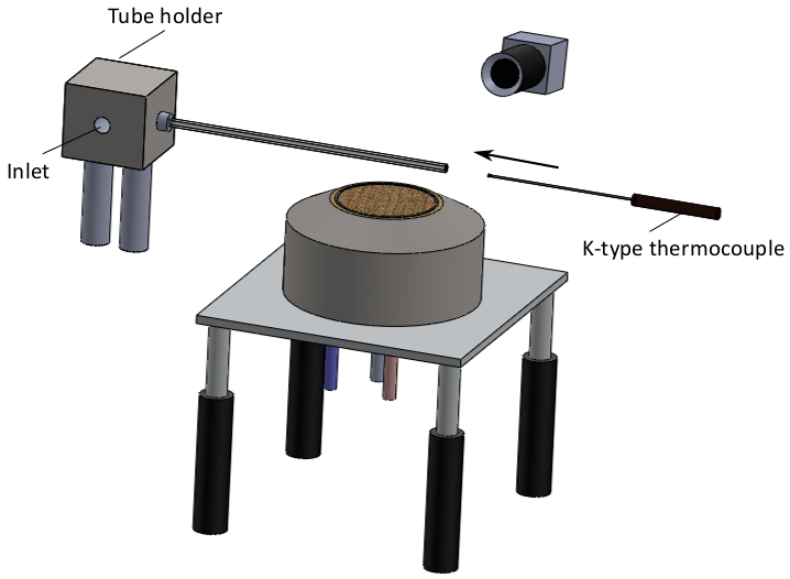

Figure 3.5: Micro reactor unit (v1.0)

mocouple motion is provided using a precision translation stage, where the measurement junction is forwarded from the cold region to the hot region while the data are acquired using a DAQ board. While translating the thermocouple, nitrogen is flown inside the tube to prevent oxidization of the tip and the translation velocity is set to 0.2 mm/s. One end of the quartz tube is attached to a tube holder which acts as reactant inlet and the other end is left open. This made the old setup applicable only for tests at atmospheric conditions, unlike the new micro reactor. The new version eliminated the use of thermocouple and is replaced by a SiC filament placed inside the quartz tube. With the SiC-pyrometry method, not only wall temperature profile but also the flame temperature measurements are obtained. Both old and new versions of micro reactor unit can be used for gaseous fuel experiments where the vaporizing unit is replaced with fuel cylinder with a gas flow controller.

3.7 Standard testing procedure (for micro reactor v2.0)

Before starting the experiments, primary reference fuels are prepared based on ASTM 2699 standards [1] where two burettes are filled with isooctane and *n*-heptane respectively and are blended on a volumetric basis. They are thoroughly mixed and stored in a vial of 22 ml. The total volume of the blend is 10 ml. The experiment procedure begins with adjusting the filament position inside the tube. In order to avoid flame shifts, the filament is positioned to the top side of the channel. After the adjustment, the filament position is confirmed by taking images from the front and the

top view with an additional (third) camera. After the filament adjustment, a cube of 1 inch side length is placed on the edge of the burner as shown in Figure 3.6. The position where the cube edge intersects the tube is calibrated as the origin. The HDR imaging sequence is then run to capture the area of interest covering the cube along with the quartz tube. To avoid stray light and background noise a dark screen is placed around the reactor.

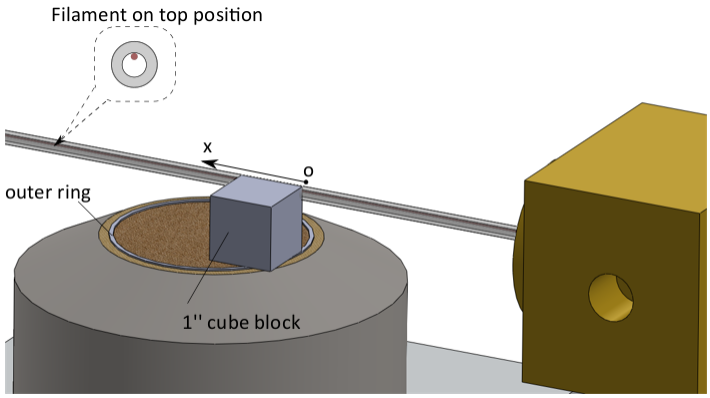

Figure 3.6: Calibration with cube block

After the cube image sequence, the external manifold is heated up to 85°C and the burner heating is initialized. The burner is ignited using a torch, which the external temperature is carefully monitored using an R-type thermocouple. To have a wider slope of temperature gradient inside the tube, an external temperature of 1600 K is chosen. This would provide a wider slope of temperature gradient on the wall which would be of good advantage when the temperature is extracted from flame position in the post processing. The desired external burner temperature is achieved gradually in steps with the burner velocity and the equivalence ratio increased from 30 cm/s- 0.3 phi to 160 cm/s-0.65 phi as shown in the+ Table 3.2. The final step with a burner velocity of 160 cm/s and an equivalence ratio of 0.65 will remain throughout the experiment to maintain the external temperature at 1600 K.

The fuel source is initially closed which the air is delivered into the tube for 3 minutes to purge the residual gases in the feed lines; the flow velocity is set to 30 cm/s. A HDR sequence is initiated to acquire images of the hot filament with air flow, which is later post processed to obtain the temperature profile. The fuel source is opened and the fuel-air mixture is maintained at stoichiometric conditions. The flow velocity is set to 80 cm/s where the stable flame regime is observed inside

Table 3.2: Burner startup parameters

Step	Burner velocity (cm/s)	Burner ϕ
1	30	0.3
3	50	0.4
4	90	0.45
5	120	0.5
6	150	0.55
7	160	0.65

the tube. The imaging sequence is launched to capture stable flames. This process is repeated for velocities ranging from 80-5 cm/s in decreasing steps of 5 cm/s to capture chemiluminescence in each combustion regime.

3.8 Concluding remarks

Unlike the old setup, the complete raw data obtained with the new setup consists of hundreds of images in 10 bit PNG format. This also includes raw data required for temperatures. The next part of the work entirely deals with image processing using Python scripts. Multi wavelength pyrometry algorithms developed by Sauer and Schoegl [24] are used as "post-processing tool" for generating temperatures from the images. Hence the next chapter gives a quick overview of post processing and discusses the results.

Chapter 4
Post Processing and Results

4.1 Introduction

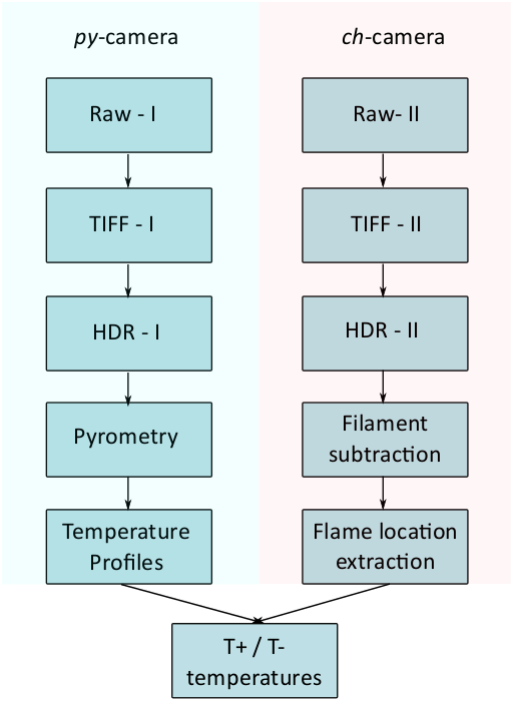

Figure 4.1: Post processing steps

After completion of an experiment with one fuel, 650-750 MB of raw image data are generated. The raw data include a set of cube images and images of the incandescent SiC filament at different mixture velocities. Each set of cube and SiC data consists of wavelength filtered images at a wide range of exposures. The post processing stage deals with the extraction of temperature profiles, flame locations, and flame ignition-extinction temperatures from the data sets. Cube images are employed for calibrating positions, whereas filament images are processed for extracting temperature profiles and flame locations. In particular, the incandescent filament images from the *py*-camera contains spectral measurements with 435 nm, 650 nm, 750 nm, 850 nm, 950 nm, and 1050 nm band pass filters, which are processed for obtaining the temperature profiles using TFP [24]. On the other hand, *ch*-camera images captured at 430 nm and 394 nm are used for extracting flame boundary locations. The wall temperatures at those extreme positions are termed $T^+$and T^-temperatures. T^+ refers to the wall temperature at the downstream position of the flame

whereas T^- refers to the wall temperature of the flame boundary at the upstream side. In case of FREI regime, $T^+$and T^- temperatures represent ignition and extinction temperatures.

Figure 4.1 shows the overall steps involved in post processing. Each set of cube and filament images are first converted into a composite high dynamic range (HDR) image before extraction. All the processing steps are performed using custom built python scripts by Sauer and Schoegl [24]. The flame locations are converted into temperatures using the wall profile to obtain non-adiabatic ignition and extinction temperatures. Figure 4.2 illustrates the extraction of $T^+$and T^-. Locations from HDR images of stable, FREI and weak flames are extracted and converted into $T^+$and T^- using the profile (shown in Figure 4.2 (b)) obtained with pyrometry.

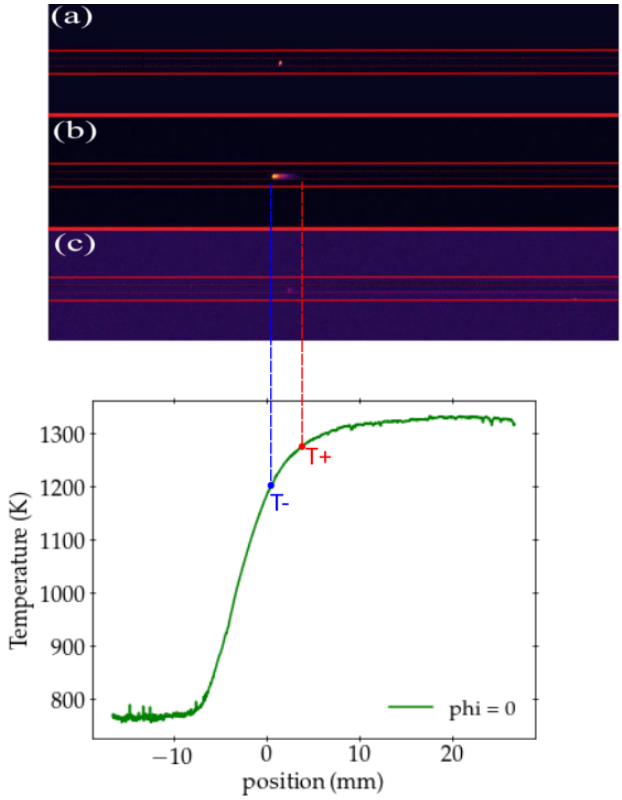

Figure 4.2: Illustration of correlating (a) HDR image of FREI to a (b) wall temperature profile

4.2 PRF results from the "old" setup (v1.0)

A translating thermocouple is used in the old setup to measure temperature profiles. Six different PRF blends are tested at 1 atm and T^+ and T^- temperatures are plotted for each mixture velocity ranging from 5 cm/s to 80 cm/s. Figure 4.3 shows ignition and extinction temperatures of isooc-

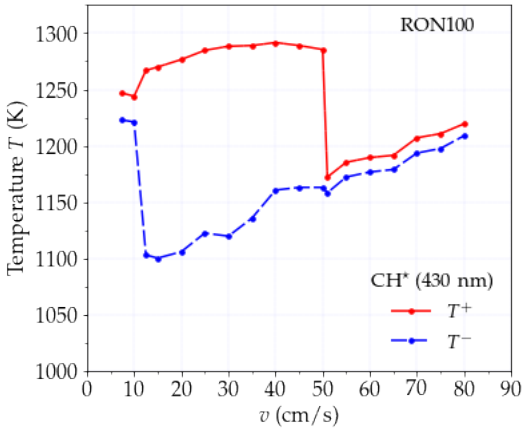

Figure 4.3: T^+ and T^- results for isoooctane at 1 atm and $\phi = 1$

tane. The red and blue lines indicate wall temperatures at the extremities of three combustion regimes. From velocities 80-50 cm/s, a narrow region between the flame boundaries is seen indicating the presence of normal stable flame. As the velocities are reduced, the stable flame shifts to the cold side. With a sudden increase in T^+ temperature, the narrow flame region gets broadened from the velocities 50-10 cm/s suggesting an ignition and extinction phenomenon. This is linked to the presence of FREI regime. The broadened region indicates the extent of FREI and its amplitude. As the velocity is reduced, the FREI extent shifts to the low temperature side. The transition from FREI to weak flames occurs below the velocities of 10 cm/s during which oscillations stop and flame stabilizes closer to the ignition locations of FREI.

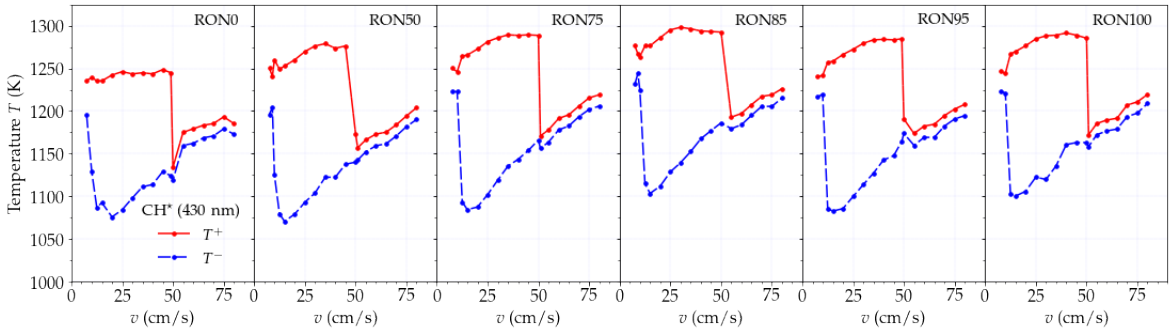

Figure 4.4: T^+ and T^- results for PRF with the old setup at 1 atm and $\phi = 1$

Figure 4.4 shows results of T^+ and T^- temperatures for all PRF mixtures. All three flame regimes are observed for each fuel and transition occurs at similar velocities i.e. FREI at 50 cm/s and weak flame at 10 cm/s. *N*-heptane shows the lowest ignition temperature compared to the rest of the fuels. From PRF 50 to PRF 85, T^+ temperatures in the FREI region exhibit a temperature increase

of 25 - 50 K. However, this trend is no longer seen for PRFs 95 and 100. No clear trend is seen in extinction temperatures of PRFs.

From the literature available on PRFs 0, 20, 50 and 100 at 1 atm [6] (Section 2.2), weak flames shift towards the high temperature side with an increase in octane number. Regardless, the shift from PRFs 50 to 100 seen in the literature [6] was low. Similar traits are observed in the current results from the old setup where the shift of T^+ and T^- is seen from PRF 0-50 and 50-100, but no large differences were observed for PRFs within the 50 to 100 range.

4.3 PRF results with the "revised" setup (v2.0)

Most of the PRFs in the former setup were concentrated near typical gasoline RON values (i.e. PRF 75, 85, 95 and 100). From the previous PRF results, it is observed that the responsiveness is low at higher RON. So in the new setup, PRFs of wide RON distribution are chosen, anticipating a good differentiation at higher RON. PRFs 0, 60, 80, 90, and 100 are tested in the new setup and the wall and flame profiles are extracted with the help of pyrometry.

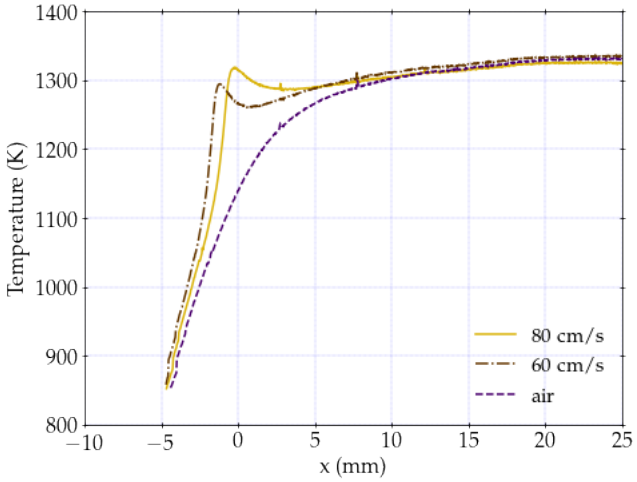

Figure 4.5: Temperature profile in stable flame region

Figure 4.5 shows stable strong flame profiles in comparison with the profile of air flowing at 30 cm/s. As the velocities decrease, peak temperatures (T_{max}) corresponding to stable flames tend to decrease and peak positions are shifted to the cold side. A similar pattern of shifts in stable flames with velocities was reported for the "old" PRF results.

A temperature profile for the FREI regime at a flow velocity of 40 cm/s is shown in Figure 4.6.

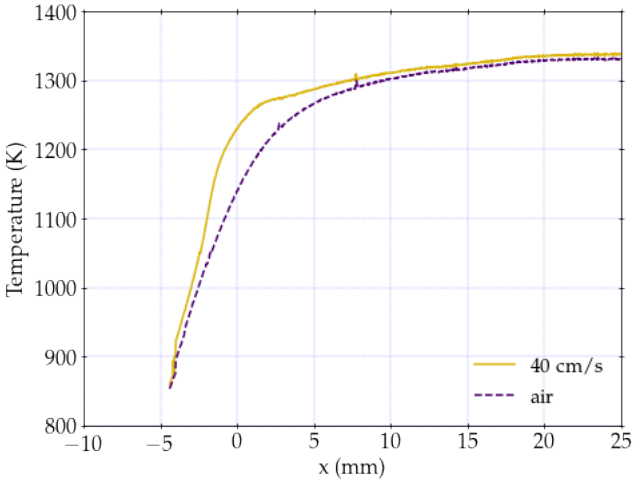

Figure 4.6: Temperature profile in FREI region

The FREI region does not exhibit a peak, instead, a wide zone with elevated temperatures is seen near the temperature gradient.

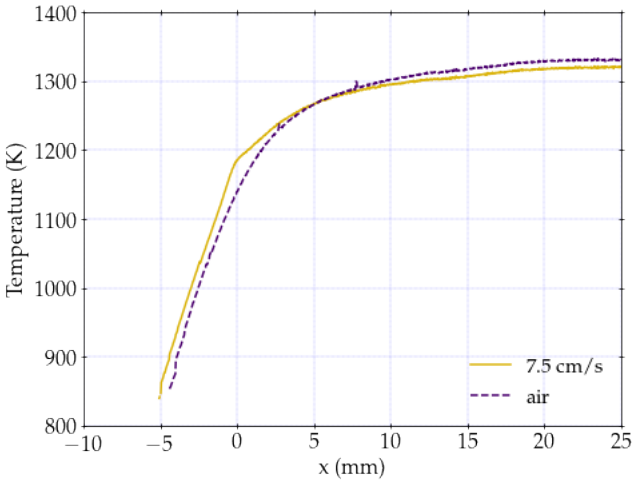

Figure 4.7: Temperature profile in weak flame region

At a velocity of 7.5 cm/s, a peak with a slight temperature rise is seen as shown in Figure 4.7, which is attributed to the presence of a weak flame. At the lowest velocities, both flame and wall temperature profile with air will coincide.

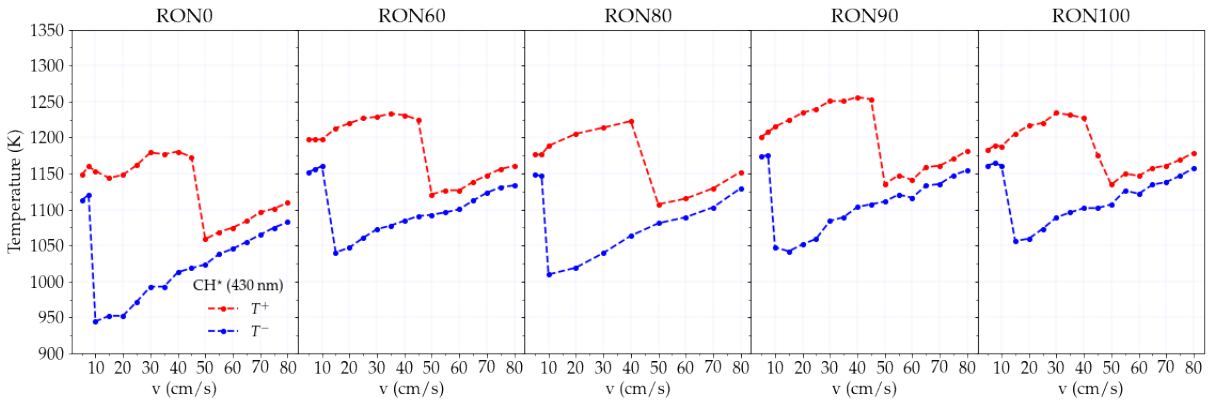

Figure 4.8: $T^+$and T^- results for PRF with the new setup at 1 atm and $\phi = 1$

Results with T^+ and T^-vs velocity are plotted again using the new setup for five different PRFs at 1 atm as shown in the Figure 4.8. The FREI regime ranges between 10-50 cm/s for all fuels. As seen previously, *n*-heptane shows the lowest ignition and extinction temperatures compared to the rest of the fuels. Similar to "old" PRF results, no clear sensitivity is seen at higher octane numbers. Due to the low sensitivity at atmospheric pressures and uncertainties involving in the experiment, clear differentiation is not evident at higher ON blends. It is also noted that T^+ and T^- temperatures from the new setup are lower than that of old results by 20-40 K. The reason is attributed to the shift in temperature profiles.

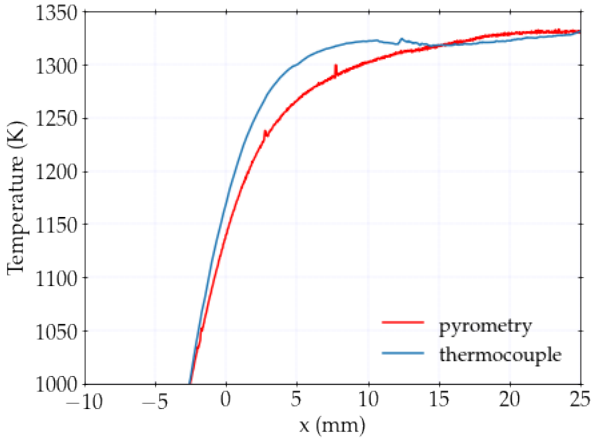

Figure 4.9: Wall temperature profiles comparision

Figure 4.9 shows the comparison of wall temperature profiles between the two measurement techniques. Both measurements have the same burner parameters of 160 cm/s and an equivalence ratio of 0.65. The largest difference is around 40 K at the gradient region.

4.4 High pressure PRF results

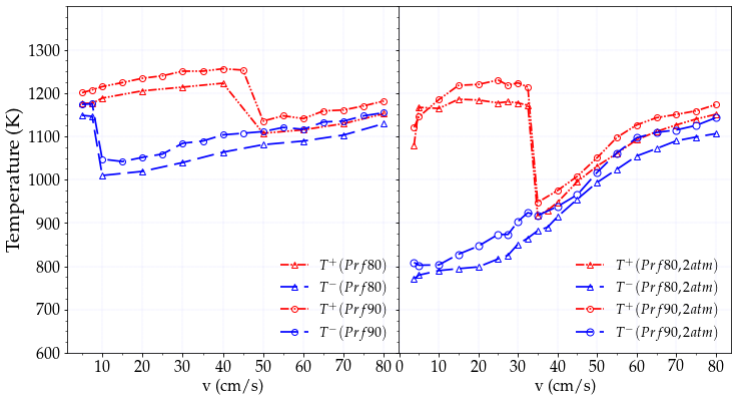

Figure 4.10: T^+ and T^- results for PRF at 2 atm and $\phi = 1$ [8]

Tests are conducted with PRF 80 and 90 at 2 atm [8] and plots comparing PRFs 80 and 90 at 1 and 2 atm are shown in the Figure 4.10. At 2 atm, FREI starts at 35 cm/s as opposed to 50 cm/s at 1 atm. It is also noted that T^- of FREI dropped to lower temperatures at high pressure. The ignition temperature of PRF 90 is higher than PRF 80 in both pressure cases. The differentiation between ignition temperatures of PRF 80 and 90 is slightly improved with an increase in pressure. However, uncertainties in temperature measurements lie within the same range as differences.

Based on literature [66], adiabatic flame velocities of isooctane-air mixtures are reduced with an increase in pressure. The transition to FREI is expected to occur at velocities lower than the laminar flame speed. This explains the transition from the stable flame to FREI for PRF 80 and 90 at lower velocities in high pressure results. It is also noted that in the FREI region, T^- temperatures for both fuels drop to lower temperatures at 2 atm. This is attributed to the increase in heat release rates (HRR) at high pressures. Due to high HRR, convection losses lead to quenching at positions farther upstream. If the pressure is increased further, quenching is expected to shift further upstream or may not occur at all.

Summing up results obtained from PRF blends,

- Results from both setup versions showed an increase in ignition and extinction temperatures from *n*-heptane to PRF 60. No clear shifts are observed for higher PRFs.

- Comparing two closely spaced PRFs (80 and 90) at 1- 2 atm, T^- dropped, and a small shift of T^+ towards high temperature is seen with an increase in pressure. However, the temperature shifts still falls within the uncertainty levels of pyrometry (30 K).

4.5 Results with TSF 89.3

So far, all experiments are conducted with different PRFs to observe ignition and extinction characteristics with different RON. Considering the fuels with high octane sensitivity, the following part of the study involves testing of fuels having different octane sensitivities. To observe the responsiveness to different MON (under same RON), TSF 89.3 and PRF 90 are tested in the micro reactor (v2.0).

Toluene Standard Fuels (TSF) are volumetric mixtures of PRFs and toluene. Table 4.1 shows specifications for TSF 89.3 and PRF 90. Though both have similar RON, TSF 89.3 possess lower MON. Tests are conducted at 1 atm and 2 atm at stoichiometric conditions. Velocities are varied from 80-5 cm/s and T^+ and T^- are extracted at each flame regime.

Table 4.1: Specifications of PRF 90 and TSF 89.3 [1, 2]

	PRF 90	TSF 89.3
isooctane vol %	90	0
n-heptane vol %	10	30
toluene vol %	0	70
RON	90	89.3
MON	90	78.2

Figure 4.11 presents the comparison of temperature data for both fuels at 1 and 2 atm. TSF 89.3 exhibits a similar extinction-ignition behavior as PRF 90 at 1 atm. At 2 atm, both fuels showed a decrease in extinction temperature as the heat release rate doubles at 2 atm. The extinction temperatures are similar in both cases at 2 atm but PRF 90 displayed higher ignition temperature with a differentiation of 30-40 K with TSF 89.3.

From results with TSF, it is observed that,

- Both TSF and PRF of identical RON showed similar T^+ and T^- at 1 atm.

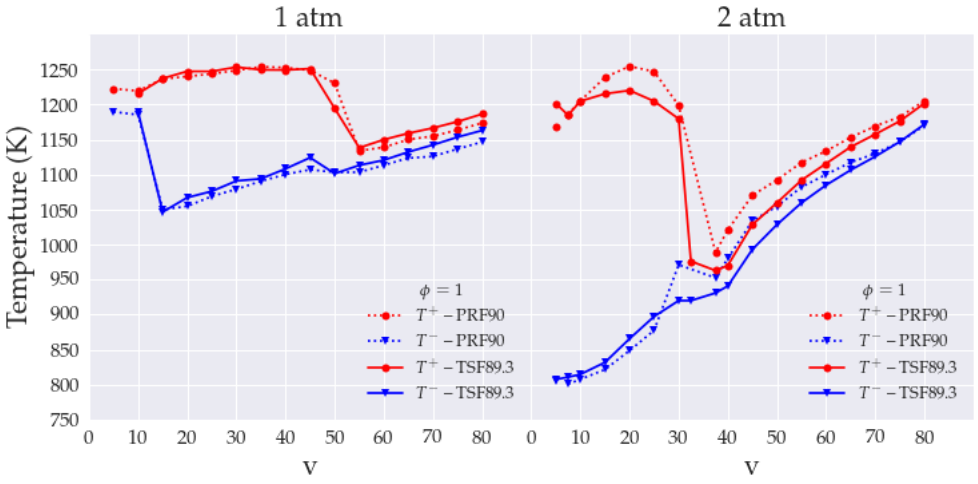

Figure 4.11: Comparison of T^+ and T^- for PRF 90 and TSF 89.3 at 1 and 2 atm, $\phi = 1$

- At 2 atm, PRF 90 (with MON 90) exhibited increased ignition temperatures compared to TSF of MON 78.2.

- From these results, there is evidence for MON relevant characteristic behavior in the micro reactor at 2 atm. To strengthen this observation, the next section presents tests results of four different gasoline fuels, one of them featuring higher MON.

4.6 Gasoline representative fuels

Table 4.2: Co-optima fuel specifications [3]

	98 RON E30	High Alkylate	High Aromatic	High Olefin
RON	98.3	97.9	98.0	98.4
MON	87.6	96.7	87.3	87.8

In the final part of this study, four real fuels/additives labeled 98 RON E30, High Alkylate, High Aromatic and High Olefin are tested in the revised micro reactor setup (v2.0) under atmospheric conditions. Each fuel is composed of fuels with different hydrocarbon chain structures. 98 RON E30 contains 30 % ethanol by volume, and by their names, High alkylate, High Aromatic and Olefin fuels contain a greater composition of alkyl (C_nH_{2n+1}), aromatic and alkene groups respectively. These fuels are developed as a part of the Co-Optimization of Fuels & Engines (Co-Optima) initiative [3] to investigate fuel dependent combustion characteristics. Table 4.2 provides RON and MON specifications for these fuels. All of them have a similar research octane rating where the

High Alkylate blend is specified with a higher MON of 96.7 compared to the rest. These fuels are tested in micro quantities using the new micro reactor setup to check the capabilities for actual fuel testing.

A distinctive behavior of the Alkylate blend is seen with $T^+$and T^- results at different mixture velocities. Figure 4.12 (a) shows combustion characteristics of fuels at different velocities, each compared with 98 RON fuel. All three combustion regimes are observed with the new fuels at similar transition phases with that of PRFs. In the FREI regime, High Aromatic and High Olefin have similar ignition temperatures with 98 RON where the differences fall below the uncertainty levels of 30K. High Alkylate, on the other hand, exhibits higher ignition temperature with 50-60 K increase compared to 98 RON.

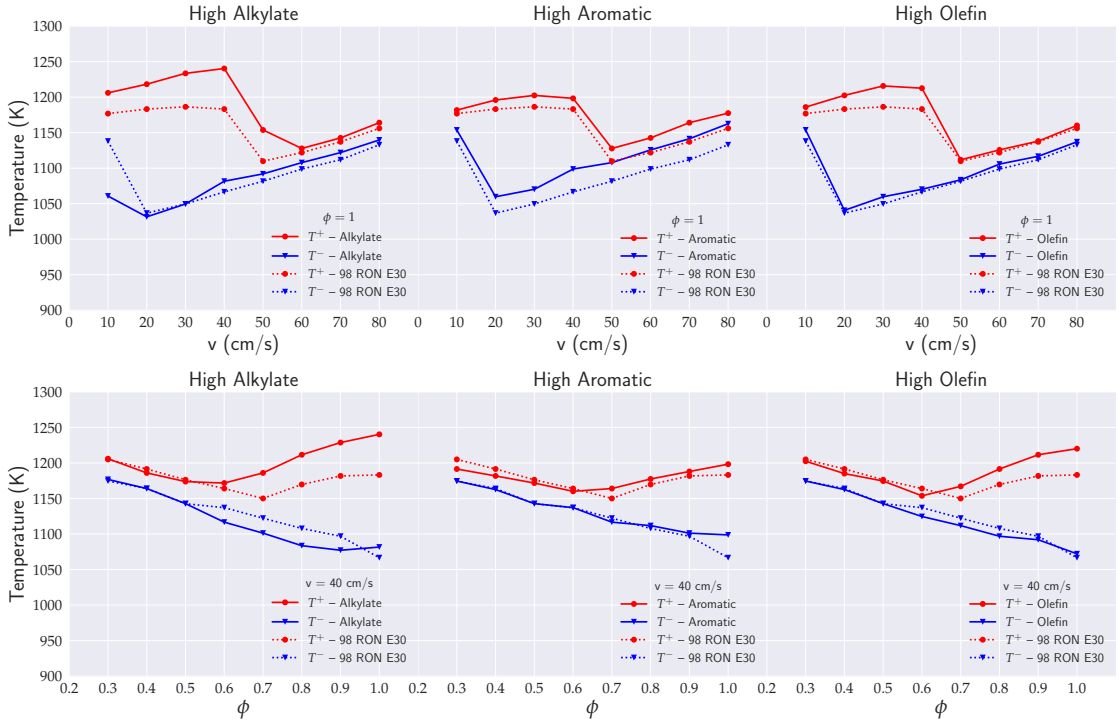

Figure 4.12: T^+ and T^- results of new fuels at 1 atm with (a) different mixture velocities at $\phi = 1$ and with (b) different equivalence ratios with v = 40 cm/s

Further fuel tests are conducted at a constant mixture velocity of 40 cm/s and the equivalence ratio is varied from 1.0 to 0.2. Results are shown in Figure 4.12 (b). The extent of the FREI region is reduced as the mixture gets leaner till $\phi = 0.6$. Aromatic and Olefin fuel show similar ignition properties as 98 RON. High Alkylate exhibits higher T^+ compared to the rest of fuels.

Based on results in the literature[33], the amplitude of FREI is reduced with a decrease in equivalence ratio. This explains a decrease of the FREI zone extent with a decrease in ϕ. High Alkylate which possess different MON exhibited distinct combustion behavior in both cases ($\phi = 1$ and v = 40 cm/s cases).

The differentiation for fuels with the same RON but with slightly different MON is observed. Based on results with gasoline fuels and TSF, there is evidence that fuel characterization w.r.t MON is possible using a micro reactor.

Chapter 5
Conclusions and Recommendations

Fuel ignition behavior plays a significant role in improving efficiencies of an IC engine. This thesis presented an alternative method of characterizing fuels using a simple micro reactor setup. Primary reference fuels which act as surrogates for gasoline were investigated in a quartz tube with a controlled temperature profile. Wall temperature measurements in the initial stages are obtained using a thermocouple; the method is switched to pyrometry in the revised version of the micro reactor setup for accommodating high pressure tests and for better spatial resolution. All three flame regimes i.e, stable flame, FREI, and weak flame were observed for different mixture velocities which agreed with literature. The impact of octane number on the flame characteristics is examined by extracting wall temperatures at the flame locations. T^+/T^- temperatures in all three flame regimes shift to higher temperatures as the octane number increases from n-heptane to PRF 50. Clear differentiation is not observed between RON 50 - 100. PRF 80 and 90 showed an increased effect on extinction temperatures at elevated pressures. Further, the transition velocity from stable to FREI regime dropped from 50 cm/s to 35 cm/s.

The final part of this study demonstrated capabilities for actual fuel testing with the setup. Four different representative gasoline fuels with the same RON but partially different MON were tested in the micro-reactor. When the velocities varied from 80 -5 cm/s, all three flame regimes were observed at transitional velocities similar to PRFs. Higher MON fuel showed somewhat higher ignition temperature compared to the fuels of same RON but lower MON. This is also observed in results of TSF 89.3 and PRF 90 at 2 atm. When the equivalence ratio is varied from 1 to 0.2 in gasoline fuels, the amplitude of FREI is reduced and the transition to weak flame occurred at 0.7 ϕ. Fuel sensitive results were also noticed with a change in equivalence ratios. Nevertheless, high pressure tests are required for better understanding of these temperature shifts.

Based on uncertainties of atmospheric tests, the next phase of the study should concentrate on pressurized experiments. The ultimate goal from this work is to employ a micro reactor as an alternative screening tool for fuels under engine relevant conditions (up to 20 bar). The author would like to suggest the following improvements and recommendations:

- Pyrometry: From results at 2 atm, it is evident that flames quench below 800 K, but the current pyrometry method can only measure accurately in the range of 850 - 1400 K. Low signal to noise ratio in the present study led to uncertainties in temperature measurement. Background noise seems to be problematic at the upstream side of the filament. Pyrometry accuracy could be improved with a camera sensor of better quality.

- Tube diameter: The results at 2 atm indicated an increase in heat release rate with extinction at 800 K. The quartz tube diameter needs to be reduced in order allow flame quenching, thereby maintaining FREI regime in the next phase of high pressure tests.

- Filament diameter: Currently a filament diameter is 75 μm is placed inside a quartz tube of 1 mm internal diameter. To accommodate tubes with diameters around 0.5 mm, the filament also needs to be scaled down for higher resolution in the filament adjustment and reduced heat re-circulation effects.

- Dilution: The heat release rate can also be controlled by diluting the fuel-air mixture with non-combustible gases such as nitrogen or other inert gases.

- Vaporization unit: In this study, heating is not required for PRFs based on Antoine's results. While the unit is heated in order to vaporize gasoline representative fuels, the fuel lines are left unheated. The setup should be updated with heated fuel lines to ensure complete vaporization at the downstream of vaporization unit.

References

[1] ASTM Standard et al. Standard test method for research octane number of spark-ignition engine fuel. *D2699, Rev. December*, 2004.

[2] D ASTM. 2700 standard test method for motor octane number of spark-ignition engine fuel. *American Society for Testing and Materials (ASTM)*, 2014.

[3] Carl Magnus Goran Sjoberg and David Vuilleumier. Co-optima core fuels: Initial investigations of knocking behavior in a disi engine. Technical report, Sandia National Lab.(SNL-CA), Livermore, CA (United States), 2016.

[4] K. Maruta, T. Kataoka, N. I. Kim, S. Minaev, and R. Fursenko. Characteristics of combustion in a narrow channel with a temperature gradient. 30:2429–2436, 2005.

[5] Yosuke Tsuboi, Takeshi Yokomori, and Kaoru Maruta. Lower limit of weak flame in a heated channel. *Proceedings of the Combustion Institute*, 32(2):3075–3081, 2009.

[6] Mikito Hori, Akira Yamamoto, Hisashi Nakamura, Takuya Tezuka, Susumu Hasegawa, and Kaoru Maruta. Study on octane number dependence of prf/air weak flames at 1–5 atm in a micro flow reactor with a controlled temperature profile. *Combustion and Flame*, 159(3):959–967, 2012.

[7] Nimal Naser, S Mani Sarathy, and Suk Ho Chung. Estimating fuel octane numbers from homogeneous gas-phase ignition delay times. *Combustion and Flame*, 188:307–323, 2018.

[8] S Navid Roohani, Veerendra Naralasetti, Pawan Sharma, Vinicius M. Sauer, and Ingmar Schoegl. Investigation of combustion characteristics of primary reference fuels in heated microchannels. 03 2018.

[9] Heather L MacLean and Lester B Lave. Evaluating automobile fuel/propulsion system technologies. *Progress in energy and combustion science*, 29(1):1–69, 2003.

[10] Rolf D Reitz. Directions in internal combustion engine research. *Combustion and Flame*, 1(160):1–8, 2013.

[11] Alex MKP Taylor. Science review of internal combustion engines. *Energy Policy*, 36(12):4657–4667, 2008.

[12] Mikael Höök and Xu Tang. Depletion of fossil fuels and anthropogenic climate change - a review. *Energy Policy*, 52:797–809, 2013.

[13] Pierre Leduc, Benjamin Dubar, Alain Ranini, and Gaëtan Monnier. Downsizing of gasoline engine: an efficient way to reduce co2 emissions. *Oil & gas science and technology*, 58(1):115–127, 2003.

[14] Ferrán A Ayala and John B Heywood. Lean si engines: the role of combustion variability in defining lean limits. Technical report, SAE Technical Paper, 2007.

[15] Robert L McCormick, Gina Fioroni, Lisa Fouts, Earl Christensen, Janet Yanowitz, Evgueni Polikarpov, Karl Albrecht, Daniel J Gaspar, John Gladden, and Anthe George. Selection criteria and screening of potential biomass-derived streams as fuel blendstocks for advanced spark-ignition engines. *SAE International Journal of Fuels and Lubricants*, 10(2017-01-0868):442–460, 2017.

[16] John B Heywood et al. *Internal combustion engine fundamentals*. Mcgraw-hill New York, 1988.

[17] Alec Groysman. History of crude oil and petroleum products. In *Corrosion in Systems for Storage and Transportation of Petroleum Products and Biofuels*, pages 221–226. Springer, 2014.

[18] GT Kalghatgi. Fuel anti-knock quality-part i. engine studies. Technical report, SAE Technical Paper, 2001.

[19] Jeffrey M Bergthorson and Murray J Thomson. A review of the combustion and emissions properties of advanced transportation biofuels and their impact on existing and future engines. *Renewable and sustainable energy reviews*, 42:1393–1417, 2015.

[20] Akira Yamamoto, Hiroshi Oshibe, Hisashi Nakamura, Takuya Tezuka, Susumu Hasegawa, and Kaoru Maruta. Stabilized three-stage oxidation of gaseous n-heptane/air mixture in a micro flow reactor with a controlled temperature profile. *Proceedings of the Combustion Institute*, 33(2):3259–3266, 2011.

[21] S. Minaev, K. Maruta, and R. Fursenko. Nonlinear dynamics of flame in a narrow channel with a temperature gradient. 11:187–203, 2007.

[22] K. Maruta, J. K. Parc, K. C. Oh, T. Fujimori, S. S. Minaev, and R. V. Fursenko. Characteristics of microscale combustion in a narrow heated channel. 40(5):516–523, 2004.

[23] Taiki Kamada, Hisashi Nakamura, Takuya Tezuka, Susumu Hasegawa, and Kaoru Maruta. Study on combustion and ignition characteristics of natural gas components in a micro flow reactor with a controlled temperature profile. *Combustion and Flame*, 161(1):37–48, 2014.

[24] Vinicius Sauer, S Navid Roohani, and Ingmar Schoegl. Toward a calibration-free multi-band multi-wavelength pyrometry using low dynamic range cmos cameras for combustion diagnostics. 03 2018.

[25] Stephen R Turns et al. *An introduction to combustion*, volume 499.

[26] Irvin Glassman, Richard A Yetter, and Nick G Glumac. *Combustion*. Academic press, 2014.

[27] Yiguang Ju and Kaoru Maruta. Microscale combustion: technology development and fundamental research. *Progress in Energy and Combustion Science*, 37(6):669–715, 2011.

[28] JH Burgoyne and H Hirsch. The combustion of methane at high temperatures. *Proc. R. Soc. Lond. A*, 227(1168):73–93, 1954.

[29] SA Lloyd and FJ Weinberg. A burner for mixtures of very low heat content. *Nature*, 251(5470):47, 1974.

[30] Lars Sitzki, Kevin Borer, Steffen Wussow, Ewald Maruta, and Paul Ronney. Combustion in microscale heat-recirculating burners. In *39th Aerospace Sciences Meeting and Exhibit*, page 1087, 2001.

[31] Nam Il Kim, Souichiro Kato, Takuya Kataoka, Takeshi Yokomori, Shigenao Maruyama, Toshiro Fujimori, and Kaoru Maruta. Flame stabilization and emission of small swiss-roll combustors as heaters. *Combustion and Flame*, 141(3):229–240, 2005.

[32] JGBF Vican, BF Gajdeczko, FL Dryer, DL Milius, IA Aksay, and RA Yetter. Development of a microreactor as a thermal source for microelectromechanical systems power generation. *Proceedings of the Combustion Institute*, 29(1):909–916, 2002.

[33] Alireza Alipoor and Kiumars Mazaheri. Combustion characteristics and flame bifurcation in repetitive extinction-ignition dynamics for premixed hydrogen-air combustion in a heated micro channel. *Energy*, 109:650–663, 2016.

[34] Taiki Kamada, Hisashi Nakamura, Takuya Tezuka, Susumu Hasegawa, and Kaoru Maruta. Study on combustion and ignition characteristics of natural gas components in a micro flow reactor with a controlled temperature profile. *Combustion and Flame*, 161(1):37–48, 2014.

[35] Mikito Hori, Hisashi Nakamura, Takuya Tezuka, Susumu Hasegawa, and Kaoru Maruta. Characteristics of n-heptane and toluene weak flames in a micro flow reactor with a controlled temperature profile. *Proceedings of the Combustion Institute*, 34(2):3419–3426, 2013.

[36] S. Suzuki, M. Hori, H. Nakamura, T. Tezuka, S. Hasegawa, and K. Maruta. Study on cetane number dependence of diesel surrogates/air weak flames in a micro flow reactor with a controlled temperature profile. 34:3411–3417, 2013.

[37] Annalisa Di Stazio, Christian Chauveau, Guillaume Dayma, and Philippe Dagaut. Combustion in micro-channels with a controlled temperature gradient. *Experimental Thermal and Fluid Science*, 73:79–86, 2016.

[38] P Grajetzki, H Nakamura, T Tezuka, S Hasegawa, and K Maruta. Evaluation of the reactivity of ultra-lean prf/air mixtures by weak flames in a micro flow reactor with a controlled temperature profile. *Combustion Science and Technology*, pages 1–21, 2018.

[39] William R Leppard. The chemical origin of fuel octane sensitivity. *SAE transactions*, pages 862–876, 1990.

[40] RF Cracknell, Johan CG Andrae, LJ McAllister, M Norton, and HL Walmsley. The chemical origin of octane sensitivity in gasoline fuels containing nitroalkanes. *Combustion and Flame*, 156(5):1046–1052, 2009.

[41] Charles K Westbrook, Marco Mehl, William J Pitz, and Magnus Sjöberg. Chemical kinetics of octane sensitivity in a spark-ignition engine. *Combustion and Flame*, 175:2–15, 2017.

[42] K Fieweger, Ro Blumenthal, and G Adomeit. Self-ignition of si engine model fuels: a shock tube investigation at high pressure. *Combustion and Flame*, 109(4):599–619, 1997.

[43] Shigeyuki Tanaka, Ferran Ayala, and James C Keck. A reduced chemical kinetic model for hcci combustion of primary reference fuels in a rapid compression machine. *Combustion and flame*, 133(4):467–481, 2003.

[44] S Mani Sarathy, Goutham Kukkadapu, Marco Mehl, Weijing Wang, Tamour Javed, Sungwoo Park, Matthew A Oehlschlaeger, Aamir Farooq, William J Pitz, and Chih-Jen Sung. Ignition of alkane-rich face gasoline fuels and their surrogate mixtures. *Proceedings of the Combustion Institute*, 35(1):249–257, 2015.

[45] Tamour Javed, Changyoul Lee, Mohammed AlAbbad, Khalil Djebbi, Mohamed Beshir, Jihad Badra, Henry Curran, and Aamir Farooq. Ignition studies of n-heptane/iso-octane/toluene blends. *Combustion and Flame*, 171:223–233, 2016.

[46] CV Callahan, TJ Held, FL Dryer, R Minetti, M Ribaucour, LR Sochet, T Faravelli, P Gaffuri, and E Rani. Experimental data and kinetic modeling of primary reference fuel mixtures. In *Symposium (International) on Combustion*, volume 26, pages 739–746. Elsevier, 1996.

[47] Mohammed AlAbbad, Tamour Javed, Fethi Khaled, Jihad Badra, and Aamir Farooq. Ignition delay time measurements of primary reference fuel blends. *Combustion and Flame*, 178:205–216, 2017.

[48] R Di Sante. Measurements of the auto-ignition of n-heptane/toluene mixtures using a rapid compression machine. *Combustion and flame*, 159(1):55–63, 2012.

[49] J Herzler, M Fikri, K Hitzbleck, R Starke, C Schulz, P Roth, and GT Kalghatgi. Shock-tube study of the autoignition of n-heptane/toluene/air mixtures at intermediate temperatures and high pressures. *Combustion and flame*, 149(1-2):25–31, 2007.

[50] JF Griffiths, PA Halford-Maw, and C Mohamed. Spontaneous ignition delays as a diagnostic of the propensity of alkanes to cause engine knock. *Combustion and flame*, 111(4):327–337, 1997.

[51] Nimal Naser, Seung Yeon Yang, Gautam Kalghatgi, and Suk Ho Chung. Relating the octane numbers of fuels to ignition delay times measured in an ignition quality tester (iqt). *Fuel*, 187:117–127, 2017.

[52] George Wm Thomson. The antoine equation for vapor-pressure data. *Chemical reviews*, 38(1):1–39, 1946.

[53] G Milazzo. Tensioni di vapore di alcune sostanze organiche a bassa temperatura. *Ann. Chim*, 46:1105–1111, 1956.

[54] Grant F Carruth and Riki Kobayashi. Vapor pressure of normal paraffins ethane through n-decane from their triple points to about 10 mm mercury. *Journal of Chemical and Engineering Data*, 18(2):115–126, 1973.

[55] Theodore L Bergman, Frank P Incropera, David P DeWitt, and Adrienne S Lavine. *Fundamentals of heat and mass transfer*. John Wiley & Sons, 2011.

[56] V Vilimpoc, LP Goss, and B Sarka. Spatial temperature-profile measurements by the thin-filament-pyrometry technique. *Optics letters*, 13(2):93–95, 1988.

[57] S Pauzin, A Giovannini, and B Bédat. Thin filament infrared pyrometry: instantaneous temperature profile measurements in a weakly turbulent hydrocarbon premixed flame. *Experiments in fluids*, 17(6):397–404, 1994.

[58] Jignesh D Maun, Peter B Sunderland, and David L Urban. Thin-filament pyrometry with a digital still camera. *Applied optics*, 46(4):483–488, 2007.

[59] Timo Joutsenoja and Rolf Hernberg. Pyrometric sizing of high-temperature particles in flow reactors. *Applied optics*, 37(16):3487–3493, 1998.

[60] Bernhard Müller and Ulrich Renz. Development of a fast fiber-optic two-color pyrometer for the temperature measurement of surfaces with varying emissivities. *Review of scientific instruments*, 72(8):3366–3374, 2001.

[61] Davide Giassi, Bolun Liu, and Marshall B Long. Use of high dynamic range imaging for quantitative combustion diagnostics. *Applied optics*, 54(14):4580–4588, 2015.

[62] Nathan J Kempema and Marshall B Long. Boundary condition thermometry using a thermographic-phosphor-coated thin filament. *Applied optics*, 55(17):4691–4698, 2016.

[63] Peter B Kuhn, Bin Ma, Blair C Connelly, Mitchell D Smooke, and Marshall B Long. Soot and thin-filament pyrometry using a color digital camera. *Proceedings of the Combustion Institute*, 33(1):743–750, 2011.

[64] Gordon B Hunter, Charly D Allemand, and Thomas W Eagar. Multiwavelength pyrometry: an improved method. *Optical Engineering*, 24(6):241081, 1985.

[65] Paul E Debevec and Jitendra Malik. Recovering high dynamic range radiance maps from photographs. In *Proceedings of the 24th annual conference on Computer graphics and interactive techniques*, pages 369–378. ACM Press/Addison-Wesley Publishing Co., 1997.

[66] Bénédicte Galmiche, Fabien Halter, and Fabrice Foucher. Effects of high pressure, high temperature and dilution on laminar burning velocities and markstein lengths of iso-octane/air mixtures. *Combustion and Flame*, 159(11):3286–3299, 2012.

Appendix A
Calibration and Pyrometry

A.1 TIFF generation and calibration

Table A.1: Image distribution in TIFF files

Filter	Py - camera	Ch - camera
395 nm	-	30
430 nm	-	30
650 nm	15	-
750 nm	15	-
850 nm	15	-
950 nm	15	-
1050 nm	15	-
435 nm	15	-
Total	90 (TIFF - I)	60 (TIFF - II)

Post processing begins with the conversion of raw images of 10 bit PNG format into a stacked Tagged Image File Format (TIFF file). TIFF is an image format used for storing lossless images such as PNG files without any compression losses. Also, several user defined information tags such as multiple exposure values and filter sequence can be included inside a TIFF file which is required for HDR conversion in later steps. Two different TIFF files are created from the images taken from pyrometry (*py*) and chemiluminescence (*ch*) cameras. Since the *py*-camera is equipped with 6 different band pass filters and 15 different exposures with each filter, the TIFF file from the first camera handles the data of 90 images. Similarly, another TIFF file stores a total of 60 images (30 and additional 30 duplicate images) from *ch*-camera which has two different filters. Table A.1 gives the overall image distribution in both TIFF files.

Composite HDR images are generated from TIFF files using python scripts with the Debevec algorithm [65]. Cube HDR images are used for calibrating positions. Common calibration standard is achieved from both cameras' cube HDR images. They are scanned and the pixel intensities are plotted. Cube detection for the HDR image in *py*-camera is shown in the Figure A.1. The boundaries of the cube are detected based on the discontinuities in the intensities. The origin and a point of 25.4 mm in the spatial domain are calibrated.

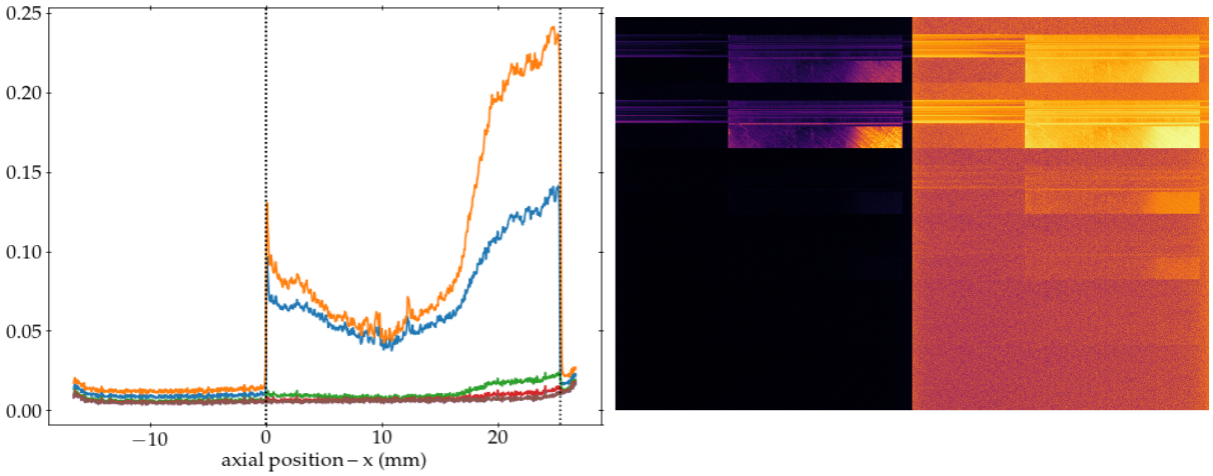

Figure A.1: (a) Cube detection and (b) HDR - I images of cube

A.2 Temperature profiles

Temperature profiles are classified as flame temperature profiles and wall temperature profiles based on the presence of flame in the channel. Wall temperature profiles are essential for determining ignition and extinction temperatures. They are obtained from the images of air or nitrogen running inside the quartz tube at 30 cm/s. Flame temperature profiles are acquired from the images of filament along with the flame. The current method employs pyrometry technique for temperatures with an incandescent filament as the target object. Temperatures are estimated using the multi wavelength multi band approach [24] (refer section 2.6). Wall and flame temperature profiles are extracted from the HDR-I images. Figure A.2 shows the extracted wall temperature profile from pyrometry with air flowing inside the tube ($\phi = 0$).

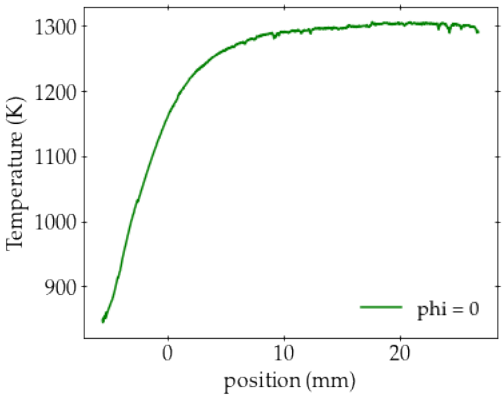

Figure A.2: Wall temperature profile extracted using pyrometry

Appendix B
Filament Processing

B.1 Filament subtraction

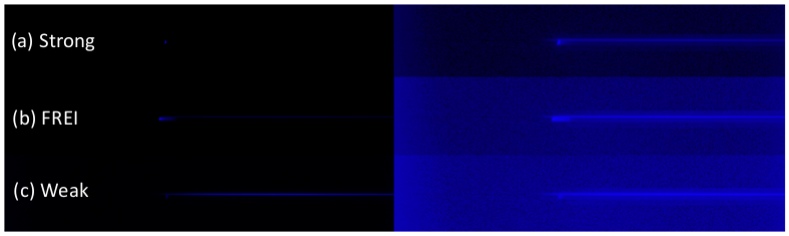

Figure B.1: HDR images of captured flame regimes

Figure B.1 shows the tone mapped HDR images of flames at 430 nm region, processed from ch-camera images. In all three cases, combustion zones can be seen. However, in the weak flame case B.1(c), the filament luminosity is dominating the chemiluminescence of the weak flame. This imposes processing complexities for acquiring the flame locations.

Filament subtraction step in the post processing stage is introduced due to the complications occurred while obtaining weak flame locations. Additional 394 nm filter is equipped to mitigate the speckles formed on the quartz tube after prolonged heating. Filament emissions are similar in both wavelength regions, but the chemiluminescence is weak in 394 nm region. A synthetic filament is calculated from the temperature profile and is used for subtracting out the filament from 430 nm image and the flame locations are determined from the resulting image. Figure B.2 illustrates the subtraction process from an HDR image with flame and filament.

B.2 Flame locations

Flame locations are determined from the filament subtracted images. The locations are detected based on a threshold value in pixel intensities. Three points are determined on a flame peak from the scripts as shown in the Figure B.3 termed as x_{ext}, x_{max}, and x_{ign}. The points x_{ext} and x_{ign} denotes the boundaries of the flame zone whereas the point where the highest intensity is seen is termed as x_{max}. In case of FREI, x_{ext} and x_{ign} denotes the extinction and ignition points. A Similar processing script will be used on the flame temperature profile for calculating "T_{max}" which indicates the characteristic flame temperature at the peak position. To obtain extinction (T^+) and ignition (T^-)

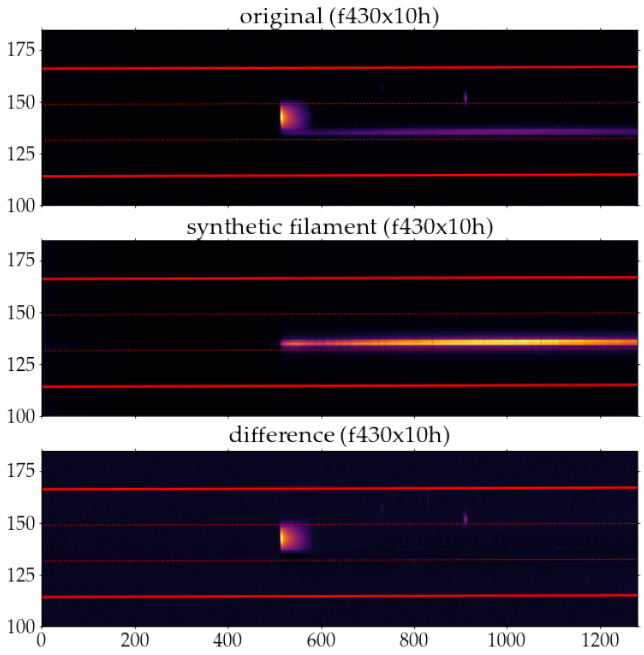

Figure B.2: Filament subtraction [8]

temperatures of the flames, locations x_{ext} and x_{ign} are correlated on to the wall temperature profile. Flame locations at each mixture velocity are determined and correlated to wall profile to obtain $T^{+}$and T^{-} temperatures.

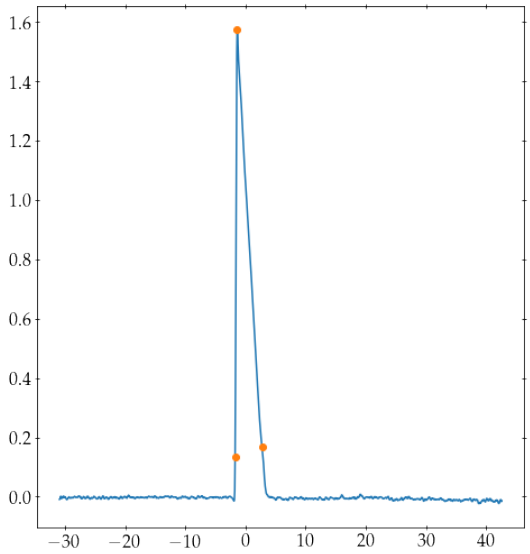

Figure B.3: Flame location points

VITA

Veerendra Naralasetti was born in Vijayawada, India. After finishing the primary and high school education in the same city, he attended Jawaharlal Nehru Technological University, Kakinada where he received his Bachelor's in Mechanical Engineering (2012-2016). Shortly after graduating, he joined in MSME program at Louisiana State University in August of 2016 taking Thermal and Fluid science as the specialization. He started his research on micro combustion under the guidance of Dr. Ingmar schoegl, and expects to graduate in August of 2018.